An Experimental Study on the Dynamic Sensitivities of Bistable Structures under Combined Stochastic and Harmonic Excitations

Undergraduate Honors Thesis

Presented in Partial Fulfillment of the Requirements for Graduation with Distinction
in the Department of Mechanical and Aerospace Engineering of The Ohio State University

By

Quanqi Dai

Undergraduate Program in Mechanical Engineering

The Ohio State University

May 2016

Thesis Committee:
Ryan L. Harne, Advisor
Jack McNamara

ABSTRACT

Multiple stable equilibria, which are static displacement configurations, are hazardous or advantageous for structures depending on the application. For example, multistable structures may exhibit snap-through dynamic response associated with large amplitude displacements between the stable equilibria. Adaptive structures could take advantage of snap-through dynamics to generate a means for large shape change and properties tuning without the requirement for continuous active controls. Alternatively, slender and thin panels on high-performance aircraft may become post-buckled such that, under extreme loading scenarios, snap-through dynamics may occur bringing catastrophic and undesired consequences, like fatigue failure. Thus, for both kind of applications the activation characteristics of snap-through dynamics in multistable structures must be characterized. Previous researchers have focused on the dynamic features of multistable systems under either deterministic or purely stochastic excitations, or have focused strictly on the unique stochastic resonance phenomenon. However, the more realistic excitation scenarios that combine harmonic and stochastic components are not well studied. In order to provide a more complete understanding of the sensitivities on the robustness and vulnerability of multistable structures to snap-through dynamics, this research establishes new experimental methods to quantify the likelihood of triggering various dynamic transitions induced in a bistable structure as a result of combined harmonic and stochastic loading. The bistable structure serves as an archetype for system with multiple stable equilibria while enabling experimentation to be conducted with greater consistency and control. According to the experimental results, the contribution of noise in the excitation with harmonic frequency near the linear natural frequency disables the persistent large amplitude snap-through dynamics. Additionally, the additive noise significantly compromises the integrity of locally stable small amplitude periodic oscillations that occur at about one-half of the linear resonant frequency. Moreover, by varying the excitation and structural parameters, this study details the sensitivities of the archetypal bistable structure according to change in the harmonic excitation frequency and amplitude, stochastic excitation amplitude, and structural design. These experimental discoveries contribute valuable insights to the practical implementation of bistable components in adaptive structures applications as well as provide informative guidance for slender vehicle component deployment under practical excitation environments.

ACKNOWLEDGEMENTS

I first and foremost thank my advisor Prof. Ryan Harne. I would never accomplish this research over the past year without his patient instruction, kindly encouragement and constant support.

I also want to thank Prof. Jack McNamara for his support and help as my committee member.

All related experiments in this research are conducted in the Laboratory of Sound and Vibration Research (LSVR) that is directed by Dr. Harne.

TABLE OF CONTENTS

LIST OF FIGURES

LIST OF TABLES

1 INTRODUCTION

1.1 Snap-through dynamics and bistable structures

Snap-through is the dynamic response associated with large amplitude displacements between the stable equilibria of bistable, multistable, or post-buckled systems, and is also termed 'interwell' response by some researchers. It is a nonlinear dynamic behavior that results in a sudden conversion between the system's potential and kinetic energy [1]. Snap-through buckling occurs in structures where stiffness decreases under the increasing loading to a limit point when structure is forced to suddenly transition to the other stable equilibria. As an example, Figure 1 shows the snap-through behavior exhibited in a bistable structure by using the load-deflection relationship [2]. Solid portion of curve demonstrates the stable structural deflections x able to be realized by application of the force $F(x)$. If the force increases from the dashed curve/blue square to beyond the limit point (yellow star in Fig. 1) the structure is triggered to lose stability of the local stable equilibrium configuration that is shown by blue square in Fig. 1. The negative stiffness region, in which lies the unstable equilibrium as shown by red circle in Fig. 1, is the reason for the sudden displacement of the structure from the yellow star. Once the force is removed, the structure returns to the other stable equilibrium given by the green square.

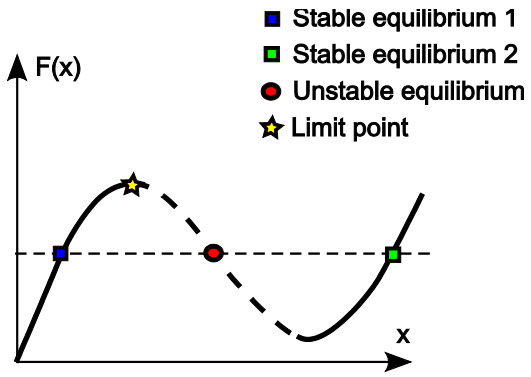

Figure 1. Bistable system force displacement relationship

Here, shows the relationship between external force, perpendicular to bistable structure, and bistable structure displacement on which point the force is acting

A *bistable structure* is one that has two stable equilibrium and one unstable equilibria due to various factors including geometric constraints, or thermal and mechanical loads [3] Bistable structures in practice include aircraft and spacecraft structures [3] and many structures containing slender elements [4] that are statically loaded in ways to result in post-buckled operation, for instance due to thermal stresses. Because multistable structures do not involve a considerable change in the types of dynamic response they may exhibit with respect to bistable structures [5], bistable structures are appropriate platforms to study the fundamental dynamic responses and sensitivities of a whole class of engineering systems that have multiple stable equilibria. In this way, bistable structures are 'archetypal' for multistable platforms. Due to existence of more than one stable equilibrium position, under harmonic external perturbations (such as pressure loads or lateral stresses) bistable structures exhibit dynamic behaviors that includes

small amplitude oscillations around one of two stable equilibria, shown in Fig. 2(a) and (b), snap-through behaviors, shown in Fig. 2(c), as well as aperiodic dynamics, shown in Fig. 2(d), which makes the investigation of bistable structure dynamic sensitivities a fascinating research topic.

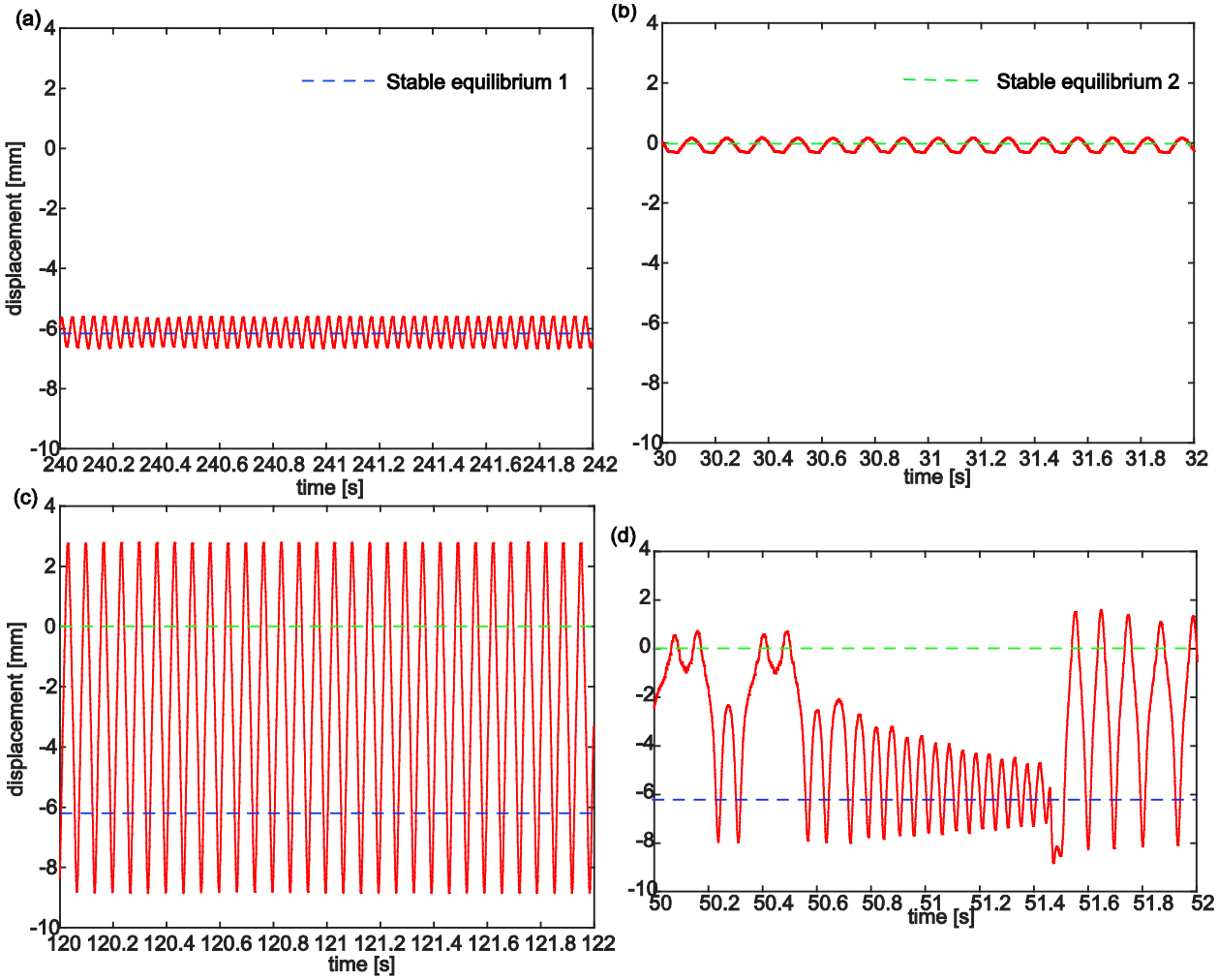

Figure 2. Experimental time series of bistable structure responses under harmonic excitation. (a) Intrawell dynamics around stable equilibria 1 (b) Intrawell dynamics around stable equilibria 2 (c) Snap-through dynamics (d) Aperiodic dynamics. Harmonic excitation frequencies slowly change at a rate of 0.08Hz/s with a constant amplitude 0.75 m/s^2.

1.2 Significance of research

Snap-through dynamics are recently found to be advantageous for numerous adaptive structures applications to improve performance and functionality. For example, snap-through dynamics could be used to enhance the energy conversion capability of vibration energy harvesting platforms due to a potential for high sensitivity to low amplitude excitation energies [6]. Harvesting energy from ambient vibrations to useful electrical power is challenging because the aim is to generate a consistent amount of energy to power small electronic devices, such as sensors. Linear oscillator-based energy harvesting platforms are found to be insufficient under common broadband excitations. Taking advantage of snap-through dynamics, the same vibration energy input may cause the bistable systems to undergo stochastic

resonance behaviors that considerably increase the power generation when compared to the output from linear energy harvesting platforms [7] [8]. Snap-through dynamics can also cause hazardous effects in structural systems. For example, snap-through between multiple equilibria could introduce high alternating stresses for metallic structures, which may lead to the fatigue failure. For example, aircraft panels subjected to the combined thermal and acoustic loading may exhibit this adverse dynamic so as to compromise the lifetime and integrity of the structure [3] [5]. Thus, studies on critically loaded aircraft structural systems have been recently motivated to find useful predictive tools for the structures' safe operation [9] [10].

1.3 Review of previous research

Previously, considerable research has been experimentally conducted to characterize the nonlinear response behaviors of bistable structures. One primary focus has been on the dynamic characteristics of buckled plates under intense random acoustic loads, in order to investigate the performance of air- and spacecraft panels under combined thermal and acoustic loads [11]. In these scenarios, intense random acoustic excitations, similar to spacecraft launch operations, were applied to study the snap-through responses exhibited in the bistable structure [12]. In contrast, Moon and Holmes [2] experimentally studied the dynamics of an archetypal bistable structure under pure sinusoidal excitation, using a cantilevered ferromagnetic beam bulked between two magnets. The idea of taking advantage of bistable structures to improve the performance of vibration energy platforms gave new motivation to experimentally study the responses of bistable structures under harmonic [9] excitations. In addition, some researchers experimentally found that a very small harmonic excitation component has a significant impact on the total response of a bistable structure that is otherwise driven by noise, a phenomenon known as stochastic resonance [13] [14]. While this brief review is by no means comprehensive, the previous research has provided adequate understanding on the dynamic behaviors to bistable structures when subjected to either harmonic or stochastic excitations, or under the intriguing stochastic resonance phenomenon, which are dynamic characteristics also manifest in the more complex multistable structures.

1.4 New contributions from this research

In the previous research, there is a common attention on either purely harmonic or purely stochastic excitation. However, it is not comparable to real world situations where purely harmonic or purely stochastic excitations rarely occur. Instead, the contribution of background noise is not necessarily negligible compared to the spectral peaks associated with harmonic response [18]. Alternatively, for certain applications with mostly random excitations, such as turbulence acting on aircraft panels, vortex shedding can occur to make the overall loading contribution on the structure include periodic components [19]. Thus, in many real world applications, structures are subjected to excitations including both periodic and noise contributions. While previous researchers have investigated the sensitivities of post-buckled structures to harmonic or stochastic excitations individually [3], the dynamic sensitivities of bistable structures under combined harmonic and stochastic excitations are not well studied. In addition, according to the discoveries about stochastic resonance [13] [14], the roles of stochastic excitation on the dynamics of bistable structures that are also driven by a harmonic excitation component are not negligible although

prior attention has only been paid to the particular case of the stochastic resonance phenomenon itself. This research is motivated to fill the knowledge gap and employs controlled, experimental methods to investigate the dynamic sensitivities of harmonically and stochastically excited bistable structures. Therefore, this research will provide key, new contributions on the understanding of the intricate dynamic sensitivities of bistable structures that operate under the full range of combinations between harmonic and stochastic loads. Due to the comparative characteristics of archetypal bistable structures to multistable structures that are becoming more prevalent in engineering applications, the new knowledge derived from this research may have broad impact in numerous contexts.

1.5 Research goal

The goal of this research is to experimentally characterize the dynamic sensitivities of bistable structures under combined stochastic and harmonic excitations. To achieve this goal, first an archetypal bistable structure that is representative of structures with more than one stable equilibrium is designed and fabricated. Then through experiments, the dynamic responses exhibited by the archetypal bistable structure under the combined harmonic and stochastic excitations are explored and evaluated according to their sensitivities respecting changes in key excitation and system parameters.

1.6 Overview of thesis

This thesis is organized as follows. Chapter 2 discusses the experimental setup of the archetypal bistable structure and describes the governing equation of motion for this platform. Chapter 3 describes the data acquisition apparatus and test methods used in the experiments, including the excitation and structural parameters investigated in this research. Chapter 4 presents the experimental results and provides numerous discussions on the experimental trends that provide new insights regarding the dynamic sensitivities of bistable structures under combined harmonic and stochastic loads. Chapter 5 summarizes the key experimental discoveries of this research and proposes future research directions.

2 ARCHETYPAL BISTABLE STRUCTURE MODEL

2.1 Magnetoelastic bistable structure

Moon and Holmes [2] showed that a harmonically-excited magnetoelastic beam may exhibit the full range of dynamical behaviors associated with bistability, including strange attractors, 'coexisting' periodic motions, initial condition dependence, and multiple stable equilibria. Similarly, in this research a magnetoelastic bistable structure is considered. Figure 3 shows a photograph and schematic of the magnetoelastic bistable structure created and examined in this research. A ferromagnetic spring steel beam (E =210 GPa, I =1.387×10^{-13} m^4, ρ=7800 kg/m^3) is clamped by an aluminum mount at one end and on the opposite end the beam free tip points to a neodymium magnet pair that is attached to the other aluminum mount. The length of the spring steel beam from clamped mount to free tip is $L = 124$ mm. The bistability of the structure is introduced by the magnet pair with position parameters δ and Δ, which makes the spring steel beam tip to statically point to either one of two stable equilibria, as shown in

Figure 1(b). The external excitations are applied through an electrodynamic shaker to which the two aluminum mounts are affixed.

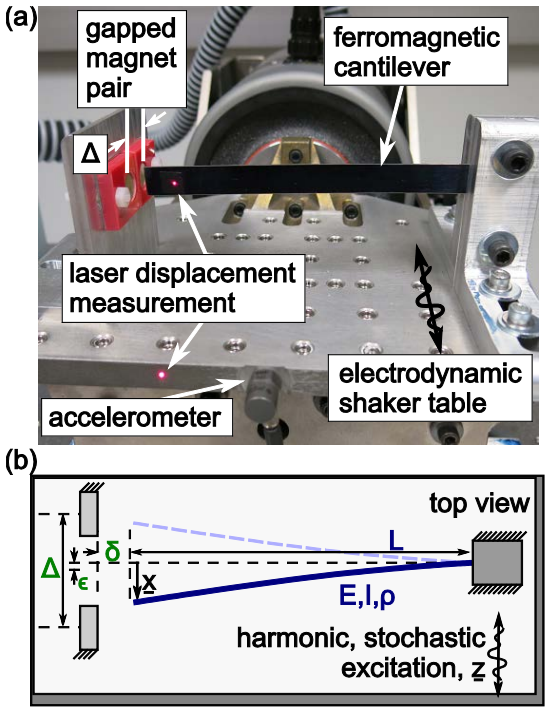

Figure 3. Overall experimental setup. (a) Photograph of experimental post-buckled cantilever and excitation method. (b) Schematic of experiment showing parameters for tuning of the bistability via magnet positioning.

The physical setup provides sufficient space to adjust the structural design, to tune structural properties, which makes it feasible to conduct substantial parameter studies. For example, the neodymium magnet pair attaches on the aluminum frame by plastic pieces which move horizontally along the channels on aluminum frame to adjust the position of magnets, shown as Fig. 4(b). Two horizontal channels on the vertical side of aluminum frame could adjust the distance between magnets as well as the offset distance (Δ and ε, using the notations in Fig. 3). While another channel on the horizontal side of the frame could change the distance (δ) from magnet pair to the free tip of spring steel beam.

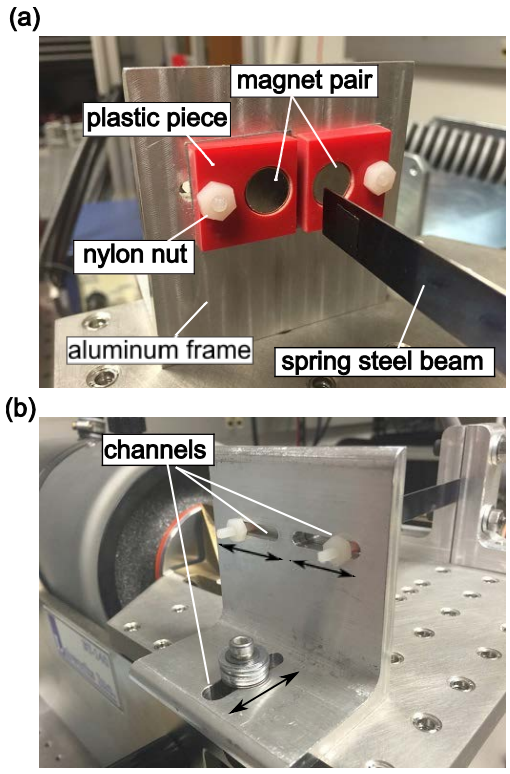

Figure 4. Photograph of zoomed out magnet pair frame. (a) Photograph of front view of magnet frame (b) Photograph of back view of magnet frame

Bistability is introduced by the magnet pair makes the ferromagnetic spring steel beam have two stable equilibria with displacement bias, as shown in Figure 5. Since the magnet space is relatively small, comparing with the distance from beam free tip to the clamped mount $L = 124$ mm, the spring steel beam is slightly buckled as shown in Fig. 5. All experimental studies in this work account for slight buckling, which is a condition known to induce only fundamental mode buckling behaviors in structural systems [20] and better enable consistent conclusions sought by these studies.

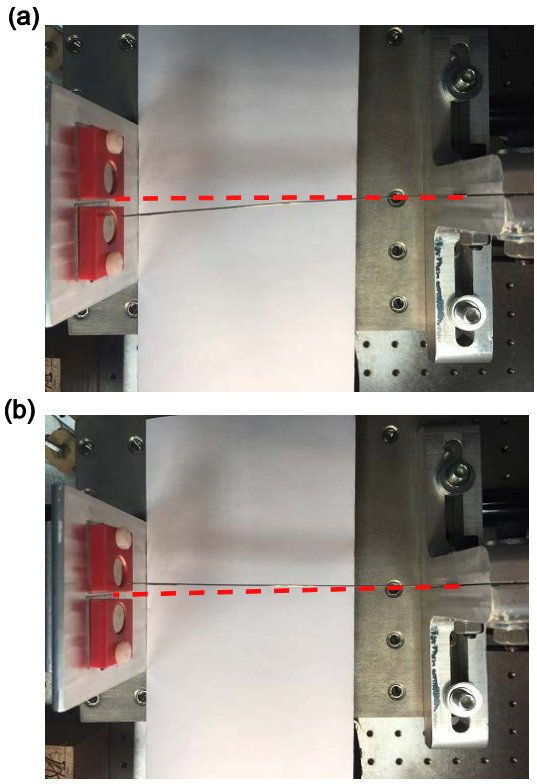

Figure 5. Photograph of two stable equilibria. (a) Photograph of top view when bistable beam is resting on equilibrium position one (b) Photograph of top view when bistable beam is resting on equilibrium position two

2.2 Governing equations for cantilever tip displacement

The governing equation of motion of the archetypal bistable structure is previously derived [21] as:

$$m\ddot{\underline{x}} + b\dot{\underline{x}} + k_1\left(1-p\right)\underline{x} + k_3\underline{x}^3 = -m\ddot{\underline{z}} \tag{1}$$

where m, b, k_1, k_3 are the principal contributions from the cantilever mass, viscous damping, linear, and nonlinear stiffness, and p is related to the nonlinear influences of the magnets that induce buckling (i.e. when $p>1$) [2] [21]. The magnetic influences also contribute to the linear and nonlinear stiffness terms k_1 and k_3 [2]. By this model formulation, the motions of the cantilever $\underline{x}$ are those directly related to the most prominent dynamic behaviors whether pre- ($p<1$) or post-buckled ($p>1$). Eq. (1) is then nondimensionalized to reduce the number of free parameters to a more compact set:

$$x'' + \eta x' + \left(1-p\right)x + \beta x^3 = -z'' \tag{2}$$

where $x = \underline{x} / l_x$ is a nondimensional length with respect to a characteristic length l_x; $z = \underline{z} / l_x$; $\omega_0 = \sqrt{k_1 / m}$ is the natural frequency prior to the buckling-related effects; $\tau = \omega_0 t$ is a nondimensional time; $\beta = k_3 l_x^2 / k_1$; and $\eta = b / m\omega_0$. The excitation includes harmonic and stochastic components

$$-z'' = F\cos\omega\tau + w(\tau) \tag{3}$$

with $w(\tau)$ given to be a Gaussian white noise process with

$$\langle w(\tau)\rangle = 0 \text{ and } \langle w(\tau)w(\tau+\tau_0)\rangle = 2\pi S\delta(\tau_0) \tag{4}$$

and S is the spectral density of the noise [22]. For the harmonic component, F is a normalized base acceleration amplitude while ω is a frequency of excitation normalized with respect to ω_0.

3 EXPERIMENTAL METHODS

3.1 Sensors, equipment, and data acquisition methods

The absolute cantilever tip displacement is measured by a Micro Epsilon ILD-1700 laser, while a Micro Epsilon ILD-2300 laser measures the displacement of the electrodynamic shaker table, with a collocated accelerometer (PCB Piezotronics 352C33). The electrodynamic shaker (LabWorks ET-140) is driven by an amplifier using a controlled signal to provide constant-amplitude acceleration at all frequencies considered in the experiments. The additional noise is controlled by prescribing the variance of an additive, normally-distributed time series of voltage that superimposes with harmonic voltage that drives the shaker. The setup of laser displacement sensors is shown in Figure 6. Two laser displacement sensors, Micro Epsilon ILD-1700 and Micro Epsilon ILD-2300 are mounted on aluminum plates and supported by a frame that is constructed by T-slots. In order to provide enough flexibility to adjust the position of laser displacement sensors, the T-slot frame and channels on the mounting plates are made to be perpendicular to each other. The direction along which sensors can move is indicated by arrows in Fig. 6.

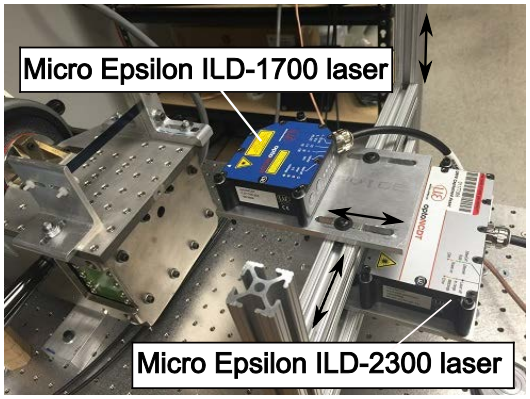

Figure 6. Photograph of laser displacement sensors and mounts

The reason to use two laser displacement sensors in this research is to indirectly measure the relative beam displacement with respect to the shaker table that used to apply eternal excitations. The main difference between these two sensors are the measuring range and resolution. Both of these two displacement can output digital and analog signals. All detailed information are demonstrated by the laser

displacement sensor instruction manuals shown in the Appendix with the sensor type used in this research highlighted.

Table 1. Comparison of laser displacement sensors

Sensor Type	Measuring range [mm]	Measuring interval			Resolution [μm]	Output types
		Start of range [mm]	Midrange [mm]	End of range [mm]		
ILD 1700-200	200	70	170	270	12	Digital/Analog
ILD 2300-200	200	130	230	330	3	Digital/Analog

In order to measure the shaker table acceleration, corresponding to the external excitation amplitude levels acting on the magnetoelastic bistable beam, an accelerometer, PCB Piezotronics 352C33, is screwed in the shaker table as shown in the photograph Fig. 3(a).

The MATLAB data acquisition toolbox is used to generate analog output signal to control the shaker and acquire analog input signal through sensors simultaneously. The sampling frequency is 2048 Hz. Once the data is acquired, all channels are digitally filtered with a low-pass filter at 200 Hz. Lastly, the cantilever tip relative displacement is computed as the difference between the beam absolute displacement subtracted from the shaker absolute displacement. An example MATLAB code used for data acquisition and post processing is shown in the Appendix.

3.2 Excitation parameters

In order to comprehensively study all potential dynamic responses and sensitivities of the archetypal bistable structure to excitation parameters, five different kinds of analog output signals are generated. Sweep harmonic frequency signals that harmonic frequencies are slowly swept from 5 Hz to 25 Hz, 240 seconds up and 240 seconds down, at a rate of 0.08 Hz/s, are applied in order to find all potential dynamics, some of which coexist under the same harmonic excitation frequency. After all potential steady-state dynamics are identified, discrete harmonic frequency signals are applied to investigate the impact of stochastic excitation, with harmonic frequencies discretely increased in 30 seconds interval for each increment within the frequency bandwidth with coexisting dynamics. By the same approach, sweep harmonic amplitude signals, discrete harmonic amplitude signals are used to study the impacts of harmonic level to the dynamic responses of bistable structure while discrete stochastic amplitude signals used to study the impact of noise level.

There are five kinds of variables needed to define each analog output signal: harmonic amplitude, harmonic frequency, stochastic amplitude, time duration, and sweep time. Table 1 catalogs these variables. In order to study the sensitivities of bistable structure to excitation parameters, the experiments

consider a significant collection of these variables through carefully controlled studies. Each kind of analog signal has controlled variables that are fixed as either zero or nonzero constant and independent variables that are either slowly swept or discretely increased. For sweep harmonic frequency and amplitude signals, the independent variables are continuously swept up and down for 240 seconds respectively in order to have a relatively slow sweep rate that assumes the structure responses at the steady-state. Due to existence of noise, discrete signals have independent variables that discretely increase with appropriate increment and a 30 seconds duration time at each increment to make sure that data is enough to conduct statistically reliable conclusions.

Table 2. Five different kinds of analog output signals

Analog output signals	*Harmonic amplitude*	*Harmonic frequency*	*Stochastic amplitude*	*Time duration*	*Sweep time*
Sweep harmonic frequency signals	Nonzero constant	Slowly sweep	Zero	–	240 seconds up and 240 seconds down
Discrete harmonic frequency signals	Nonzero constant	Discretely increase	Nonzero constant	30 seconds	–
Sweep harmonic amplitude signals	Slowly sweep	Nonzero constant	Zero	–	240 seconds up and 240 seconds down
Discrete harmonic amplitude signals	Discretely increase	Constant	Nonzero constant	30 seconds	–
Discrete stochastic amplitude signals	Nonzero constant	Nonzero constant	Discretely increase	30 seconds	–

3.3 Processes to apply excitations with swept harmonic frequency

The reason to use sweep harmonic frequency and amplitude excitations is to find all potential steady-state dynamics exhibited by the bistable structure, especially when they coexist. A group of experimental results serve as an example to illustrate how sweep harmonic frequency excitations are conducted in the experiment to find all potential dynamics, Figure 7. The displacement amplitudes shown are the result of fast Fourier transforms across brief durations of the long sweep signal. Theoretically, bistable structures exhibit intrawell oscillations and snap-through dynamics, which has been introduced in Sec. 1.1. In order to discover all those dynamics, sweep harmonic frequency excitations should be conducted at least twice. First time, the bistable structure response naturally follows the several coexisting states according to the increasing and decreasing frequency sweeps, as shown in Fig. 7(a). The black dashed (solid) arrows indicate the beam displacement amplitudes correspond to frequency sweep up (down), which shows a large overlap. When harmonic frequency sweeps down, displacement amplitude has an apparent coexisting portion with the results when frequency sweeps up. During the second run of sweep harmonic

frequency excitation, manual perturbations are needed to uncover additional coexisting responses. Fig. 7(b) shows the results under the second run. The arrows likewise indicate displacement amplitude change correspond to different frequency sweep directions, while highlighted red arrows demonstrate the impact of manual perturbations that give the beam a slight impulse to trigger random transient behavior between snap-through and intrawell. When frequency sweeps up to certain level manual perturbation triggers bistable structure generate snap-through dynamics, producing a huge increase in the harmonic displacement amplitude. As the frequency keep increases snap-through dynamics cease naturally and bistable structure goes back to small amplitude intrawell oscillations. When frequency sweeps down bistable structure under goes basically the same amplitude intrawell dynamics so the displacement amplitudes are overlapped with results when frequency sweep up. When frequency keep decreases manually perturbation, again, triggers snap-through dynamics that also cease when harmonic frequency sweeps down to low level and goes back to intrawell dynamics. The key point for running the second sweep harmonic frequency excitation is to manually perturb the bistable structure, triggering snap-through dynamics in order to find the cutoff frequencies when snap-through naturally ceases. Appropriate perturbation time is crucial to catch all the snap-through dynamics exhibited, which is achieved in this experiment by having some overlapped snap-through portion when frequency sweeps up and down. Finally, the overall potential responses are plotted in Fig. 7(c), some overlapped points could be dropped due to the repeated measurements. Notice that at the points when the beam is perturbed, there may occur responses that do not have the same displacement amplitude as intrawell dynamics, which is due to the transient behaviors caused by manual perturbations which require time to decay prior to returning to steady-state motions.

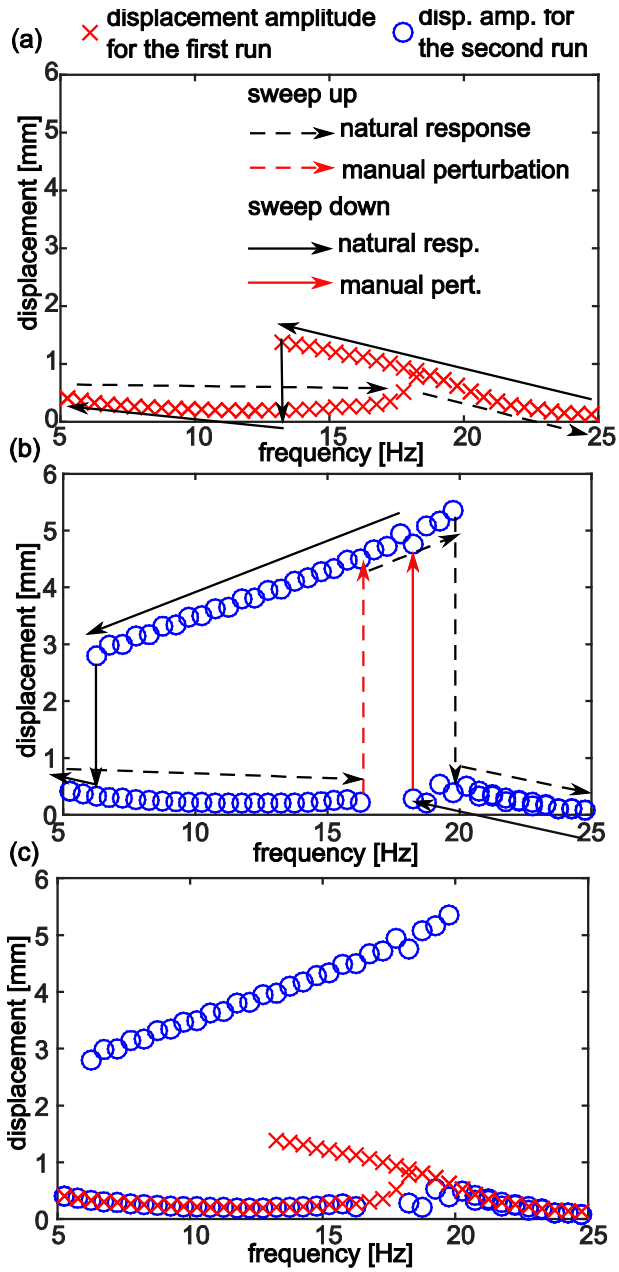

Figure 7. Bistable structure displacement amplitude under sweep harmonic frequency excitation. Here, (a) shows the displacement amplitude for first run of sweep harmonic frequency excitation without manual perturbation (b) shows displacement amplitude for the second run of sweep harmonic frequency excitation with manual perturbations (c) shows the combined displacement amplitude of two runs of sweep harmonic frequency excitation

3.4 Processes to apply excitations with discretely changing variables

In order to investigate the impact of additive stochastic excitation component on the dynamic behaviors of bistable structure, three kinds of combined harmonic and stochastic excitations are applied with discretely increasing harmonic frequencies, harmonic amplitude and stochastic amplitude, respectively. Due to the addition of noise, the bistable structure is perturbed from steady-state responses. Thus 30-second-long

time intervals are used for each discrete increment to collect statistically significant results. A snapshot of bistable structure responses in time series under discrete harmonic frequency excitation is shown in Figure 8 as an example. In order to make sure that bistable structure non-periodically generates snap-through and intrawell dynamics, manual perturbations are required to trigger the beam from one form of dynamics to other. Manual perturbations would cause some transient in the time series response, as shown by red arrow in Fig. 8.

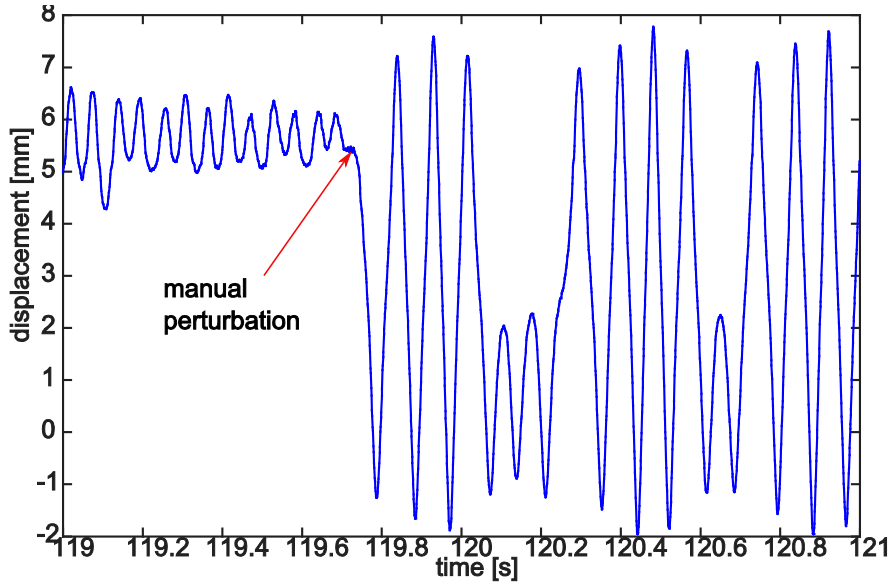

Figure 8. Snapshot of time series responses under discrete harmonic frequency excitation. This snap-shot responses is when harmonic amplitude is equal to 0.75 m/s^2, stochastic variance 1 [m/s^2]^2, and harmonic frequencies at 8 Hz (from 119 s to 120 s), and 9 Hz (from 120 s to 121 s).

Actually, when apply excitations with noise and discretely changing variables, manual perturbations may be frequently needed. Thus the perturbation times are recorded by using a push button switch as shown in Figure 9. Each time the beam is perturbed, the switch is pushed simultaneously to count perturbation times in number as well as their location in time.

The perturbation times do not significantly affect the overall responses following the evaluation of the responses measures such as the fast Fourier transform or mean-square displacement. Compared with the forcing cycles during each 30 seconds time interval, the manual perturbations account for less than 4 percent of the excitation cycles, which is shown by Figure 10. Fortunately, under some excitation conditions, the structure responds in all of the coexisting dynamics due to the noise itself serving as a trigger, and thus does not require manual perturbations.

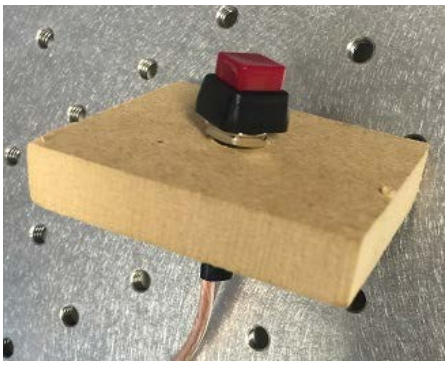

Figure 9. Photograph of momentary push bottom switch

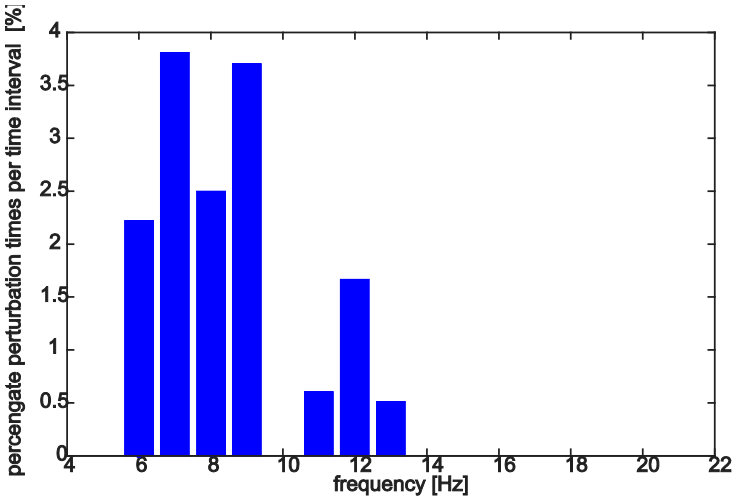

Figure 10. Manual perturbation times counting for discrete harmonic frequency excitation

3.5 Structural parameters

Two main structural parameters studied in this research are magnet space and asymmetric offset distance, (Δ and ε respectively, using the Fig. 3(b) notation). As shown in Eq. (1), the magnetic influences contribute to the linear and nonlinear stiffness terms k_1 and k_3 [2] and parameter p [2] [21]. In order to investigate the structural sensitivities to those two kinds of structural parameters, three different levels of distance are used for magnet space (Δ = 17.07 mm/ 18.50 mm/ 19.82 mm) and two different levels of asymmetric offset distance (ε = 0.63 mm/ 1.23 mm) as variables in the experiments.

3.6 Measuring natural frequency and damping ratio

As has mentioned in the previous section, structural parameters define the nonlinear stiffness of bistable structure. Thus the modification of structural setup will also change the natural frequency as well as the damping ratio, which are measured by ring-down tests. A small impulse is applied on the bistable beam when it rests at a stable equilibrium, letting it generate small amplitude intrawell oscillations which decay in amplitude in time. One example ring-down is shown in Figure 11. The log decrement method is used to

calculate damping ratio and local damped natural frequency around one stable equilibria under certain structural setup. Here, as the free response shown in Fig. 11, magnets are set to be asymmetric so bistable structure at two stable equilibrium potions should have different natural frequencies and damping ratios. Thus, in this case, two ring-down tests are required. The natural frequency and damping ratio calculated using log decrement method according to the responses shown in Fig. 11 are 23 Hz and 0.0505, respectively.

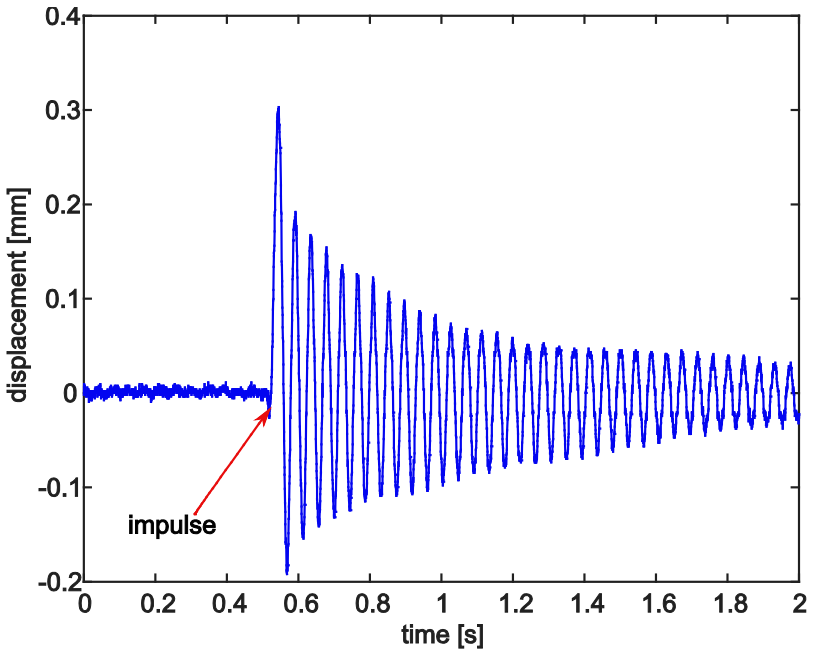

Figure 11. Free response of bistable structure around one stable equilibria after apply an impulse. Here, magnet pair is set to be asymmetric with 18.35 mm magnet distance and 1.23 mm offset (Δ =18.35mm, ε =1.23 mm)

4 RESULTS AND DISCUSSIONS

4.1 Impacts of harmonic excitation frequency

Although the influences of harmonic frequency and amplitude on the dynamic responses of bistable structures have been experimentally [23] and computationally [2] studied, the role of additional stochastic excitation upon the periodicity and robustness of bistable structures' dynamic have not been well investigated apart from specialized studies focused on the stochastic resonance phenomena [13] [14].

In order to find all potential dynamics that an archetypal bistable structure exhibits prior to the addition of noise, a sweep harmonic frequency signal is applied. Fig. 12 presents experimental results obtained for the case when the magnets are spaced symmetrically from the centerline, ε=0, such that the local linear natural frequency of beam oscillations around a stable equilibrium is about 20 Hz. As controlled variables, noise amplitude is set to be zero and harmonic acceleration amplitude controlled at 0.75 m/s^2. The excitation frequency is slowly swept from 5 Hz to 25 Hz, 240 seconds up and 240 seconds down, at a very slow rate of 0.08 Hz/s, in order to find all potential dynamics and make sure the beam responds at

steady-state. The measurements of harmonic displacement amplitude of the beam tip (from a fast Fourier transform computation) are presented in Fig. 12(a) as the black circles, while (b) shows the corresponding mean-square displacement. It is a well-known characteristic that bistable structures have coexistent dynamics for the same structural and harmonic excitation parameters [16]. Such results are demonstrated by the new measurements in Fig. 12(a), from the 6 Hz up to 22 Hz: more than one response occurs at the same harmonic excitation frequency, and for a short frequency band around 15 Hz even three dynamics coexist. The larger displacement amplitude dynamic is the persistent snap-through dynamics while the two displacement amplitudes with lower values correspond to intrawell oscillations of the beam tip around one of the locally stable equilibria, putting the model results back into context. As the harmonic frequency increases, the snap-through dynamics have an increasing displacement amplitude and suddenly cease, while the displacement amplitudes of intrawell oscillations progressively become smaller as the harmonic frequency increases beyond the linear natural frequency. Fig. 12(c) shows the corresponding percentage of time that the beam spends snapping through per excitation cycle. Since the beam responds at steady-state under the sweep harmonic frequency excitations, the results must be either 0 or 1, which is evident in Fig. 12(c) for the absent of noise results (black circles).

In order to find the impacts of noise, discrete harmonic frequency signals are used with the same structural setup, and controlled variables, harmonic acceleration amplitude is fixed at 0.75 m/s^2 and noise with standard deviation 1 m/s^2. The harmonic frequency is discretely increased from 5 Hz to 20Hz with 0.5 Hz increment and 30 seconds time duration for each increment. Because the additional noise perturbs the beam's steady-state responses, it is not possible to observe the coexisting dynamics based on the experimental data when the noise level is sufficient in the relevant frequency bandwidth. Thus as expected only one resulting data point appears at each excitation frequency in the measurement as shown in Fig. 12 as the red squares. According to experimental results in Fig. 12 (red squares), the introduction of noise significantly changes these trends. For example, as shown in Fig. 12(a), at low harmonic frequencies the displacement amplitude is significantly decreased, comparing with the snap-through dynamics in the absent of noise. In addition, the displacement amplitude appears to have a trend that first goes up then goes down as the excitation frequencies increase, and the maximum measured displacement response occurs for an excitation frequency of about 11.5 Hz, Fig. 12(a), which is about 55% of the natural frequency, 20 Hz. In fact, this excitation frequency corresponds to the greatest percentage of time that the beam spends snapping through per cycle, Fig. 12(c).

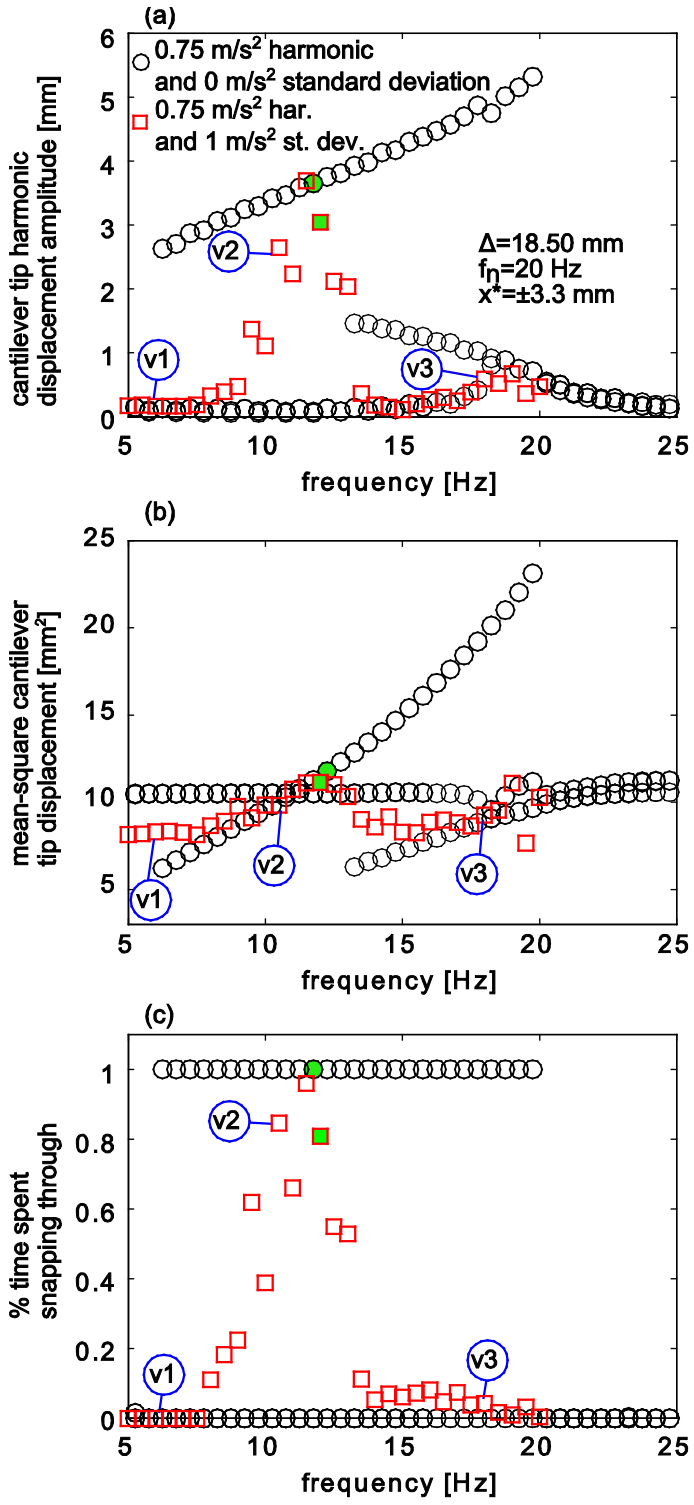

Figure 12. Experimental measurements of bistable structure response as a function of variation in the harmonic excitation frequency. Here, (a) shows harmonic displacement amplitude, (b) shows mean-square displacement, and (c) shows percentage of time that the beam spends snapping through per 30-second stationary excitation. As a function of variation in the harmonic excitation frequency.

Further insights are sought by evaluating the beam displacement responses in time series at 12 Hz, using the truncation of measured data corresponding to individual points highlighted in Fig. 12 with green fill/shading. Figure 13 shows a snapshot of the time series measurements corresponding to (black dot-dashed) steady-state snap-through oscillations without noise and (red solid) harmonic and stochastic vibrations when the noise contributes to the excitation.

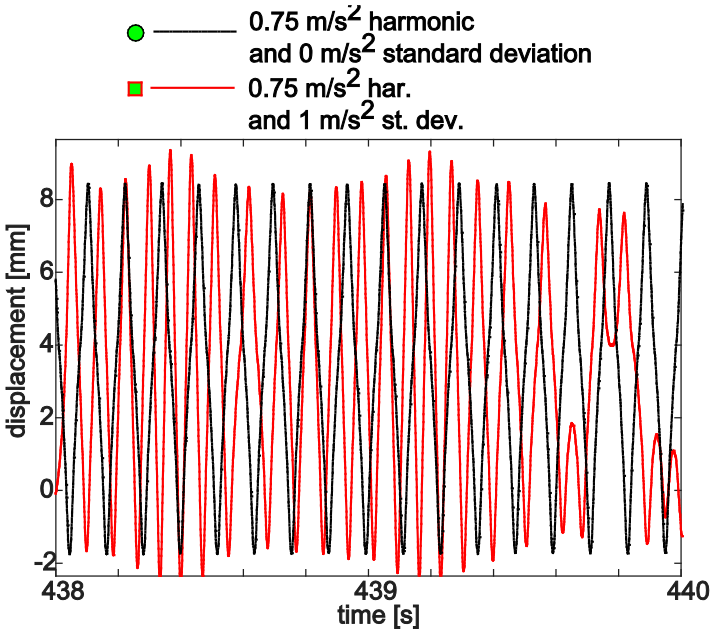

Figure 13. Time series of displacements measured without (black dash) and with (red solid) additive noise under harmonic excitation amplitude 0.75 m/s^2 at 12Hz.

As shown in Fig. 13, the introduction of noise reduces the percentage of time that the beam snaps through, which agrees with the data in Fig. 12(c). This result also agrees with the expectation that additional noise may reduce the periodicity of responses. However, it is surprising to notice that displacement amplitudes under excitations with noise have peaks that are even larger than the snap-through responses under pure harmonic excitations. It is surprising because from the displacement amplitude measurement, shown in Fig. 12(a), the overall displacement amplitude after taking a FFT computation for 360 forcing cycles (30 seconds time duration, at 12 Hz) shows that the amplitude of snap-through dynamics under pure harmonic excitations should be larger than dynamics under excitation with noise. In addition, the instantaneous phase of the dynamic trajectory with noise (red solid) in Fig. 13 is constantly changing, which is apparent when compared to the unchanging phase of the persistent snap-through oscillations in the case without noise (black dashed). This is the evidence that additional stochastic energy contributions reduce the integrity of beam's steady-state, snap-through dynamic responses, significantly disabling their persistence. As shown in Fig. 12(c), at higher harmonic frequency region, nearing the structure's natural frequency the time percentage that the beam able to snap-through is very low.

More evidence about the dynamic sensitivities to harmonic excitation frequency is acquired by examining portions of the displacement time series for the points labeled as v1, v2, and v3 in Fig. 12. Using the phase-lag-based phase portrait [1] where T is the harmonic excitation period, the characteristics of the trajectories are plainly assessed. As shown in Fig. 14(a), the bistable structure response under small harmonic excitation frequency is represented by trajectory v1 as the consolidation of the oscillations to a small region. In addition, the dominant frequency of this response is not the harmonic excitation frequency, instead the bistable structure is more effectively driven by the stochastic excitation component to respond at the fundamental natural frequency around 20 Hz (or around 3.2 times the harmonic excitation frequency, 6 Hz). This observation is supported by the evidence of corresponding autocorrelation and autospectrum plots in Fig. 14(b) and (c) as black dash curves. In contrast, as the harmonic excitation frequency increase, the bistable structure response labeled v2 reveals a snap-through dynamic with large displacement amplitude and more appreciable autocorrelation of the structure response when shifted by integer numbers of the excitation period, as shown by red dot-dash curves in Fig. 14. According to the autospectrum in Fig. 14, the response is dominated by the harmonic excitation frequency instead of the structural natural frequency. Yet, the noise still contributes greatly to the total response that the autocorrelation plots shows a rapidly decaying similarity of values as the time shift increases, Fig. 14(b). One interesting trend shown in the autocorrelation plots is that at about every $5i$ excitation periods (where $i = 1, 2, ...$) the v2 trajectory has the greatest similarity with respect to the preceding cycle of oscillation, which could be a sign of a time-dependent dynamic sensitivity for the snap-through response under combined harmonic and stochastic excitation. Finally, the trajectory v3 in Fig.14 exhibits only occasional snap-through, resulting in an autocorrelation trend with a fading non-zero bias, in contrast to the sinusoidal-like characteristics more often attributed to the autocorrelation of periodic dynamics.

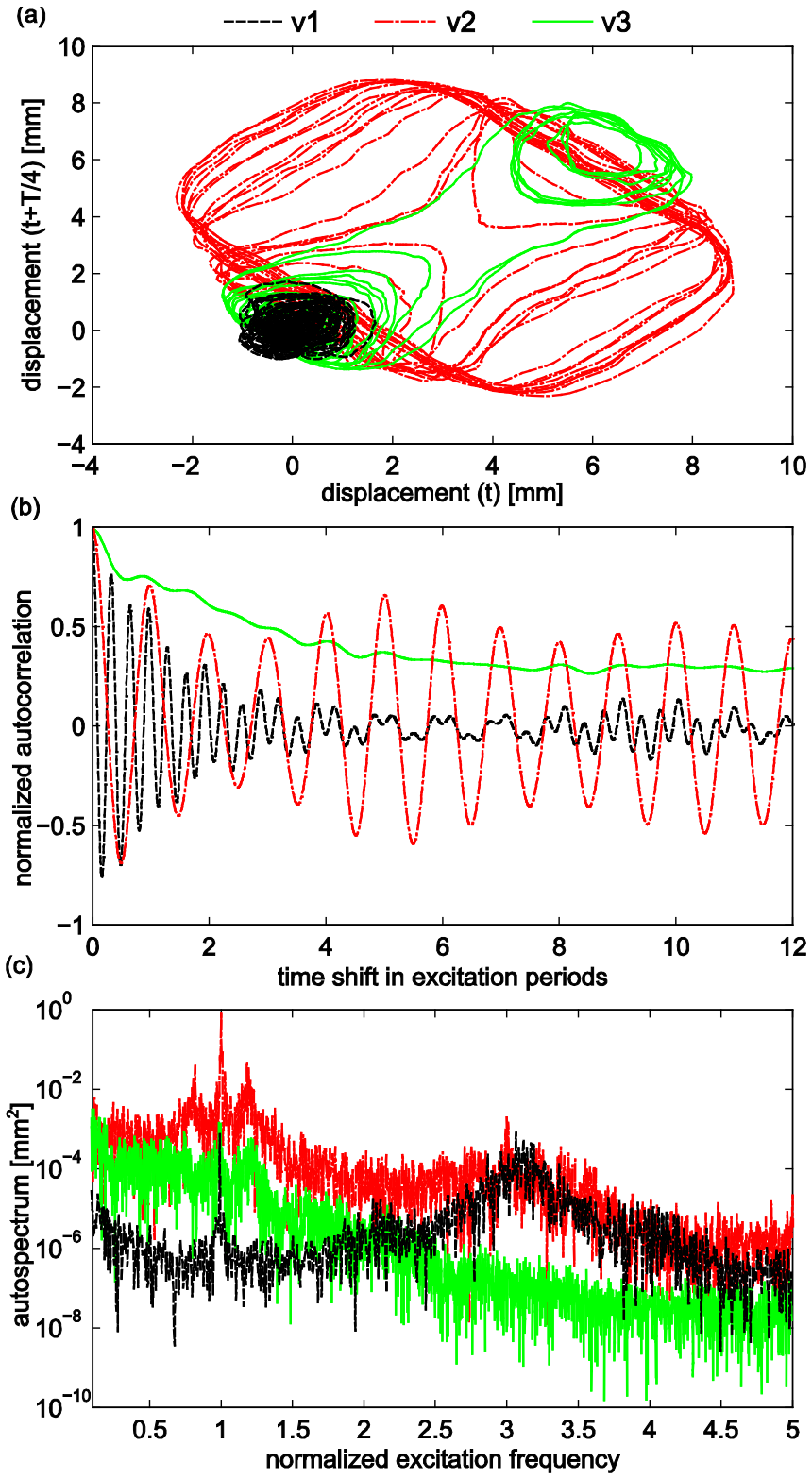

Figure 14. Portions of time series recordings of beam displacement as indicated by the labels v1, v2, and v3 in Fig. 12. Here, (a) shows a phase-lag phase portrait of the beam displacement response for a portion of this time series span, (b) shows the autocorrelation of the the corresponding data point, and (c) shows the autospectrum of the corresponding data point.

Thus, based on these findings, coexisting snap-through dynamics near the beam natural frequency are effectively disabled by the stochastic excitation component. On the other hand, snap-through dynamics occurring at about 55% of the structural natural frequency are readily promoted by the additive noise. These results provide guidance when using bistable structures in applications that hope to leverage the snap-through dynamics, like energy harvesting platforms [6], operating at the structures' natural frequency won't have an efficient power generation because stochastic perturbations from excitation would inhibit snap-through. Instead, one should design the energy harvesting platform so that the harmonic excitation frequency is about 55 percent of structure's linear natural frequency. Then as described above, through the evidence of experimental results, bistable structure would exhibit robust snap-through dynamics, thus have a high performance and efficient power generation when subjected to real world excitations.

4.2 Impacts of harmonic amplitude

Based on previous research results, harmonic excitation amplitude is shown to have a significant influence on the dynamic responses of bistable oscillators [16]. However, the stochastic excitation influences upon the otherwise harmonic responses are not clearly identified, outside of the unique case of stochastic resonance [13] [14]. In order to study the influences of harmonic amplitude to the dynamic behaviors of bistable structure, a sweep harmonic amplitude excitation is applied to first find all potential dynamics during the harmonic amplitude interval studied in this research. Figure 15 presents the experimental results of harmonic excitation amplitudes, proportional to shaker table acceleration, and sweep from 0 to 1.161 m/s^2, with controlled variables excitation frequency and noise level set to be 12 Hz and zero respectively. Fig. 15(a) shows the measurements of harmonic displacement amplitude of the beam tip as black circles. The lower branch with smaller displacement amplitudes are results corresponding to intrawell dynamics, while the upper branch with larger displacement amplitude are corresponding to persistently snap-through responses. As shown by Fig 15(a), the small amplitude intrawell dynamics happen from the lowest excitation level, while the large amplitude dynamics start at certain level of harmonic excitation, and from excitation level $0.3m/s^2$ more than one response occurs at the same harmonic excitation level. Previous research has proved the robustness of dynamic responses that bistable oscillator exhibits to changes in excitation level [16]. The same conclusion could be drawn by the evidence from experimental results that both intrawell and snap-through branches show consistent displacement amplitudes over large range of harmonic excitation amplitudes, as shown by black circles in Fig. 15(a). The corresponding percentage of time that the beam spends snapping through per excitation cycle is shown in Fig. 15(b). Since under the sweep harmonic amplitude excitations beam has steady-state responses, the results for percentage snap-through time must be either 0 or 1, which is evident in Fig. 15(b) for the absent of noise results (black circles).

In order to study the impact of stochastic excitation, discrete harmonic amplitude excitations are applied with fixed 12 Hz harmonic frequency and 1 m/s^2 noise standard deviation, while harmonic amplitude is discretely increased with 30 seconds time duration for each increment. It is not possible to experimentally observe the coexisting dynamics due to the significance of the noise level compared to the harmonic

amplitudes. Thus only one data point appears at each excitation amplitude in the measurement as shown in Fig. 15 as the red squares. The introduction of noise to the excitation significantly alters the response of bistable structure, as shown by red squares in Fig. 15. For example, in Fig. 15(a) as the harmonic excitation amplitude increases the displacement amplitude also increases. The similar trend with the percentage snap-through time by forcing cycle, shown in Fig. 15(b), that as the excitation amplitude increases the beam has larger likelihood to have snap-through dynamics. These results are intuitive that the increasing harmonic amplitudes enlarger the amount of external excitation energy, thus increase the dynamic response's amplitude as well as the likelihood to generate large amplitude dynamics.

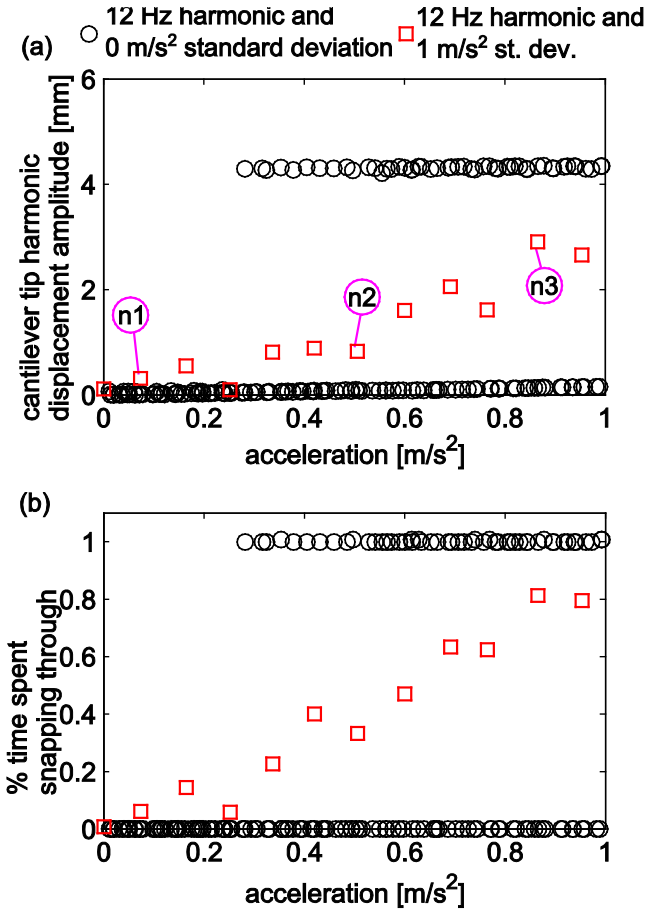

Figure 15. Experimental measurements of bistable structure response as a function of variation in the harmonic excitation amplitude. Here, (a) shows harmonic displacement amplitude, (b) shows mean-square displacement, and (c) shows percentage of time that the beam spends snapping through per 30-second stationary excitation. As a function of variation in the harmonic excitation amplitude.

Further insights about how harmonic excitation amplitude impacts the bistable beam displacement amplitude are sought by plotting the beam displacement against itself one quarter of cycle later, as shown in Figure 16. This kind of time-lag embedding plot reconstructs the phase space of responses that correspond to labeled points n1, n2, n3 in Fig. 15. When the harmonic excitation amplitude is small,

results in Fig. 16 shown by trajectory n1 (black dash curve) indicate that there is a strong influence of the underlying intrawell response such that the phase trajectory is concentrated around a stable equilibrium. The red dash-dot curve in Fig. 16 shows the trajectory corresponding to the point labeled as n2 in Fig.15. As the harmonic amplitude increases the phase trajectory encloses a larger area, and instead of around only one static equilibria at zero displacement the phase trajectory also includes the other stable equilibrium position at beam displacement about 6 mm, which demonstrates that beam occasionally undergoes snap-through response. When harmonic excitation level becomes even higher, responses shown by trajectory n3, the enclosed area in phase projection becomes larger, as shown by green solid line in Fig. 16, which indicates that beam has even larger amplitude responses, now entirely accounting for a snap-through dynamic. According to these results, increasing harmonic acceleration amplitude starting from the level when only locally small amplitude intrawell oscillation occur will increase the responses displacement amplitude, and end up with large amplitude dynamics.

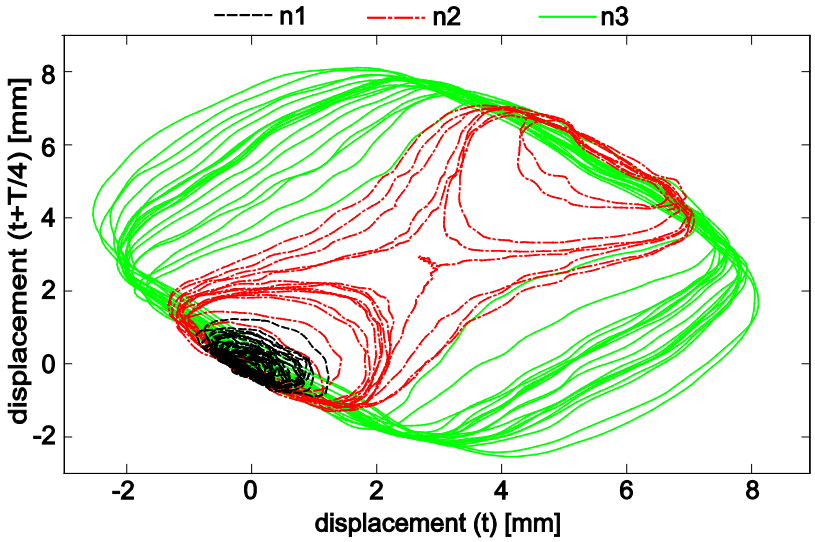

Figure 16. Time-lag phase portrait of the beam displacement response as indicated by the labels n1, n2, and n3 in Fig. 15(a) for a portion of this time series span

More evidence about the harmonic excitation amplitude influence is shown in Figure 17 by autocorrelation and autospectrum plots of dynamic responses according to labeled points n1, n2 and n3 in Fig. 15. As shown in the autospectrum Fig. 17(b), the black dash trajectory n1 demonstrates negligible peaks at the harmonic excitation frequency. Instead the beam is driven by the stochastic excitation component to respond at the fundamental natural frequency around 18 Hz (or 1.5 times the harmonic excitation frequency, 12 Hz). Comparatively, the trajectory n2 has an autocorrelation trend with decreasing non-zero bias as shown in Fig. 17(a) due to the inconsistent snap-through dynamics that result is occasional intrawell behaviors corresponding to both stable equilibrium (and hence displacement biases). In addition, similar to the autospectrum n1, the dominate frequency of dynamics corresponding to n2 is still not the harmonic excitation frequency. Finally, n3 reveals snap-through dynamic responses with more appreciable autocorrelation values at integer numbers of excitation period time shifts. However, the

stochastic excitation component still indicates a great contribution to the total response, which is shown by the fading ‘memory’ in the decaying autocorrelation as the time shift increases.

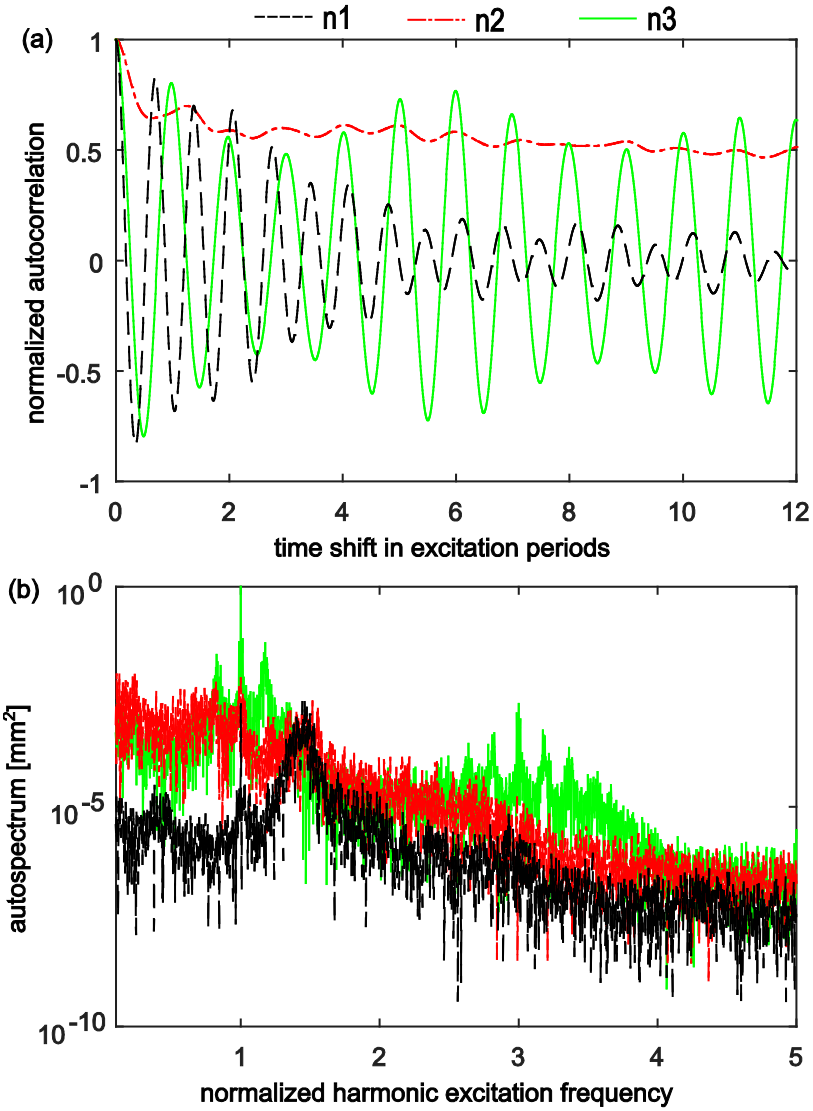

Figure. 17 Autocorrelation (a), and autospectrum (b) of the beam displacement response as indicated by the labels n1, n2, and n3 in Fig. 15(a) for a portion of this time series span

According to these findings, when snap-through coexists with the intrawell response regime, the increase in harmonic excitation amplitude enhances the probability to trigger the large amplitude snap-through dynamics as well as the robustness of snap-through dynamics, for very high levels of harmonic excitation with respect to the noise level. However, when the harmonic excitation level is very low the responses of bistable structure appears to reduce to mostly-stochastic behaviors that are spectrally dominated by the fundamental natural frequency, which is also shown in the results in section 4.1 when study the impacts of harmonic frequency.

4.3 Impacts of stochastic amplitude

The stochastic excitation component has been shown to provide noticeable impacts on the bistable structure dynamic response in section 4.1. Further investigations are conducted to characterize the influences of different levels of stochastic excitation. Since the additional Gaussian white noise changes the steady-state periodic dynamics to aperiodic dynamics, it is not possible to experimentally capture steady-state responses for many moderate to high levels of noise. In order to study the impacts of different stochastic levels on the dynamic behaviors of bistable structure, several combined harmonic and stochastic excitations are applied, with discretely increasing stochastic amplitude, but fixed harmonic amplitude and frequency. Figure 18 presents the experimental results of different stochastic amplitudes, represented by acceleration standard deviation, on the dynamic behaviors of bistable structure. The harmonic excitation frequency is set to be 12 Hz while the harmonic amplitudes are set at different levels, 0.69 m/s^2, 1.58 m/s^2. Fig. 18(a) shows the measurements of displacement amplitude of the beam tip (from a fast Fourier transform computation), for two harmonic levels, and fig. 18(b) presents the corresponding percentage snap-through time per forcing cycle. As shown by Fig 18 the existence of noise change the displacement amplitude uniquely based on the harmonic excitation amplitudes. Red circles represent results using a small harmonic amplitude, 0.69 m/s^2. As the acceleration standard deviation increases the displacement amplitude increases, and percentage snap-through time increases, starting from 0, as well. Once the standard deviation of the noise increases substantially enough, low amplitude intrawell responses under goes a sudden transient to have snap-through dynamics, which is shown by red circles Fig. 18(b). On the contrary, the measurements with high harmonic amplitude, 1.58 m/s^2 (blue triangles) have a decreasing trend for both displacement amplitude and percent snap-through time as the acceleration variance increase. Similarly, those trends have a sudden drop when noise amplitude is above certain level.

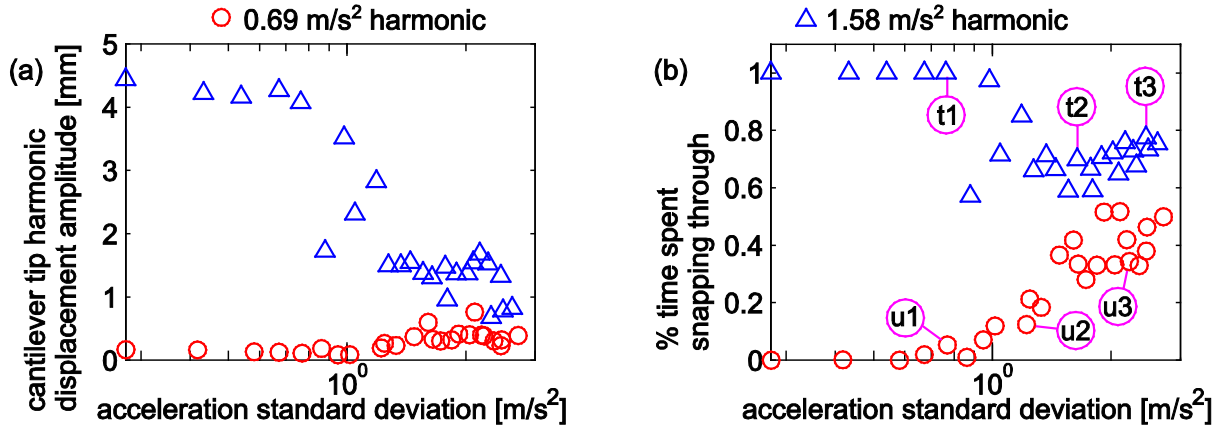

Figure 18. Experimental measurements of bistable structure response as a function of variation in the base acceleration standard deviation for two levels of harmonic acceleration. Here, (a) shows harmonic displacement amplitude and (b) shows percentage of time that the beam spends snapping through per 30-second stationary excitation. The harmonic excitation frequency is 12 Hz, and the magnet positioning parameter is Δ =17.66 mm.

According to these experimental results, as the noise level is sufficient enough to perturb the beam from its steady-state, a sudden noticeable change occurs in the dynamic responses. Explanations for this observation are gained from the phase-lag-based phase portrait and autocorrelation of responses that correspond to data points labeled as u1, u2, and u3 in Fig. 18(b). Time-lag embedding plot reconstructs the phase space of responses, while autocorrelation establishes the repeatability of a signal [1]. The black dash trajectory u1 in Figure 19(a) is the beam response when stochastic excitation deviation is low, which corresponds to point labeled u1 in Fig. 18(b). Results show that response is a periodic oscillation around one stable equilibrium. These kind of intrawell oscillations are at the linear natural frequency instead of the harmonic excitation frequency, which can be proved by the autocorrelation function that the second highest similarity is about 0.64 time shift of 12 Hz excitation period, indicating that the response is at 18.75 Hz that is close to 19 Hz natural frequency. Results with greater noise contribution to the excitation, shown by u2 trajectory (red dash-dot line), indicates that some transient jumps between different dynamic regimes occur, demonstrating different displacement bias for two stable equilibrium that a bistable structure possesses. As the stochastic level further increases, results shown by green solid curve u3, responses approach a steady-state large amplitude dynamic. According to the autocorrelation function in Fig. 19(a), at large stochastic level response is at the harmonic excitation frequency, despite the fading bias associated with imperfect persistence of the snap-through behavior. The increasing stochastic level change the dynamic responses from intrawell oscillation with primary response at the linear resonant frequency to snap-through dynamic behaviors exhibiting nearly the same harmonic frequency as the excitation. These findings suggest that when harmonic excitation amplitude is low, an increase in noise level changes the responses from stochastic oscillation at linear resonant frequency to dynamic behavior with nearly the same frequency as harmonic excitation component, which is an experimental observation of stochastic resonance. As the consequence of stochastic resonance, not only does the beam respond primarily at the same frequency as harmonic excitation component, but it also exhibits a larger displacement amplitude and increasing likelihood to snap-through, as shown in Fig. 18 by red circles.

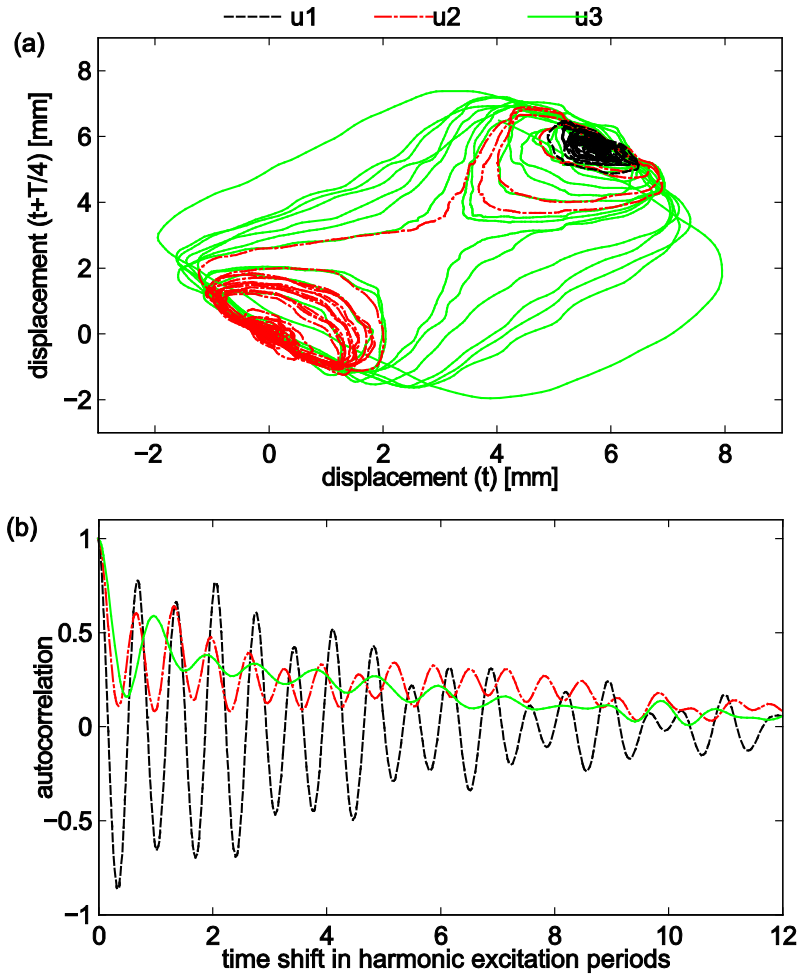

Figure 19. Portions of time series recordings of beam displacement as indicated by the labels u1, u2, and u3 from Fig. 18(b). Here, (a) shows a phase-lag phase portrait of the beam displacement response for a portion of this time series span, while (b) shows the autocorrelation of the corresponding data point.

According to experimental results, the increase in percentage of time that the beam spends snapping through is observed for standard deviations of noise around 1.3 m/s^2 and greater, which is approximately twice the harmonic amplitude of the excitation. In other words, the ratio between the standard deviation of noise when the sudden increase of snap-through dynamics happen and the harmonic excitation amplitude is about 2:1. Although not suggestive of a general rule of behavior, these results do provide a guideline, based on case study, regarding this important ratio of excitation parameters.

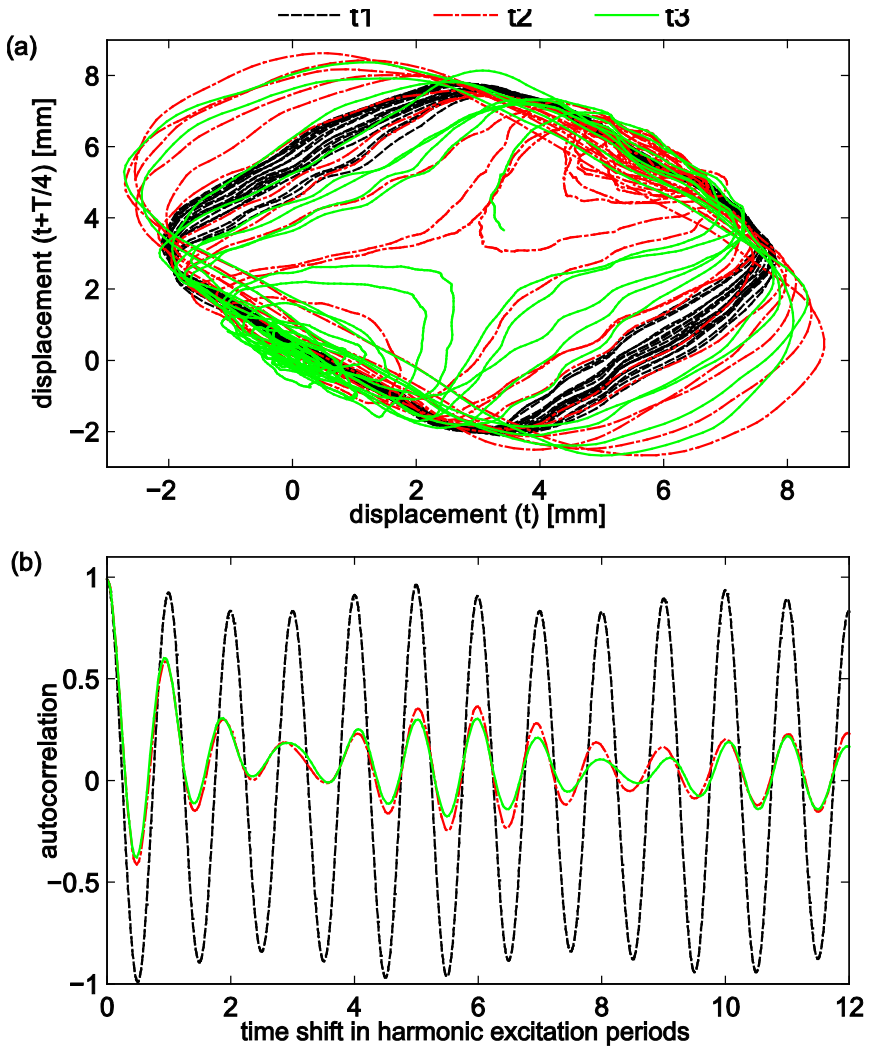

Figure 20. Portions of time series recordings of beam displacement as indicated by the labels t1, t2, and t3, from Fig. 18(b). Here, (a) shows a phase-lag phase portrait of the beam displacement response for a portion of this time series span, while (b) shows the autocorrelation of the corresponding data point.

Alternatively, under large harmonic amplitude excitation when the beam is nearly persistently snapping through, the stochastic level can impact the responses by perturbing periodic large amplitude dynamics to reduce the dynamic amplitude and periodicity, which is shown by the evidence from the autocorrelation and phase portrait plots in Fig. 20. The responses with the small noise standard deviation, as shown by point labeled t1 in Fig. 18(b), has black dash trajectory t1 shown in Fig. 20, demonstrates nearly persistent snap-though dynamics that has a very consolidated phase portrait and high repeatability at every integer time period shift on autocorrelation plot. After noise standard deviation is beyond 0.9 m/s^2 displacement amplitude and percentage snap-through time has a sudden drop according to Fig. 18(b). Thus it is expected that responses correspond to point t2 and t3 have a compromised response amplitude and repeatability that is shown in Fig. 20(b). The ratio of standard deviation of stochastic excitation when the sudden transient happen to the harmonic excitation amplitude is about 1:1.76, which is approximate the inverse ratio when stochastic excitation component causes a sudden occur of snap-through dynamics from

persistently intrawell. In addition, despite that the overall repeatability reduced a lot, responses t2 and t3 still indicate a same high similarity after 5 period shift of harmonic excitation, as shown in Fig. 20(b), which may again indicate the time-dependent dynamic sensitivity of snap-through dynamics under combined harmonic and stochastic excitations similar to the results shown in section 4.2.

4.4 Impacts of symmetric magnet positioning: symmetric bistability

Because the magnet influences contribute to the linear and nonlinear stiffness terms k_1 and k_3 [2] in Eq. (1), change in the magnet positioning parameters governs the fundamental frequency sensitivities and static equilibria of bistable structures. In order to experimentally study the impacts of the magnet positioning upon the dynamic responses of the bistable structure, different magnet spaces and asymmetric offset distances, as structural variables, are appropriately chosen. This section presents the experimental findings based on change in symmetric magnet spaces Δ, while the impacts of asymmetric offset distance ε are discussed in the next section.

The three columns in Figure 21 correspond to the experimental results for three different magnet spaces, Δ=17.07mm, Δ=18.50mm, Δ=19.82mm, respectively. The sweep harmonic frequency signal is applied to first find all potential, coexisting dynamics correspond to structural setup with three different magnet spaces Δ, as described above. As controlled variables, noise amplitude is set to be zero and harmonic amplitude controlled at 0.75 m/s^2, while excitation frequency is slowly swept. The measurements of harmonic displacement amplitude of the beam tip are presented in the first row of Fig. 21 by (a1), (b1), and (c1) as black circles, while the plots on the second row show the corresponding mean-square displacement. Similar dynamics trends are shown for three different magnet spaces by plots in the first row of Fig. 21, namely that coexistent steady-state dynamics may occur across key bands of the harmonic excitation frequency. Moreover, comparing with small magnet space Δ=17.07mm, when the magnet space increases the frequency bandwidth that snap-through dynamics may occur becomes narrower. For the magnet space Δ=18.50mm, snap-through dynamics may be activated from about 6 Hz to 20 Hz, as shown in Fig. 21(b1); while when Δ=19.82mm, the frequency bandwidth for snap-through reduce to about 6 Hz to 18 Hz, as shown in Fig. 21(c1). These trends are evidence that greater magnet space reduces the harmonic frequency bandwidth for bistable beam to generate snap-through behaviors. Moreover, these results show that the magnetoelastic structure is highly tunable in its effective structural design making it well suited for the purposes of this study as the archetypal structural system with more than one stable equilibrium.

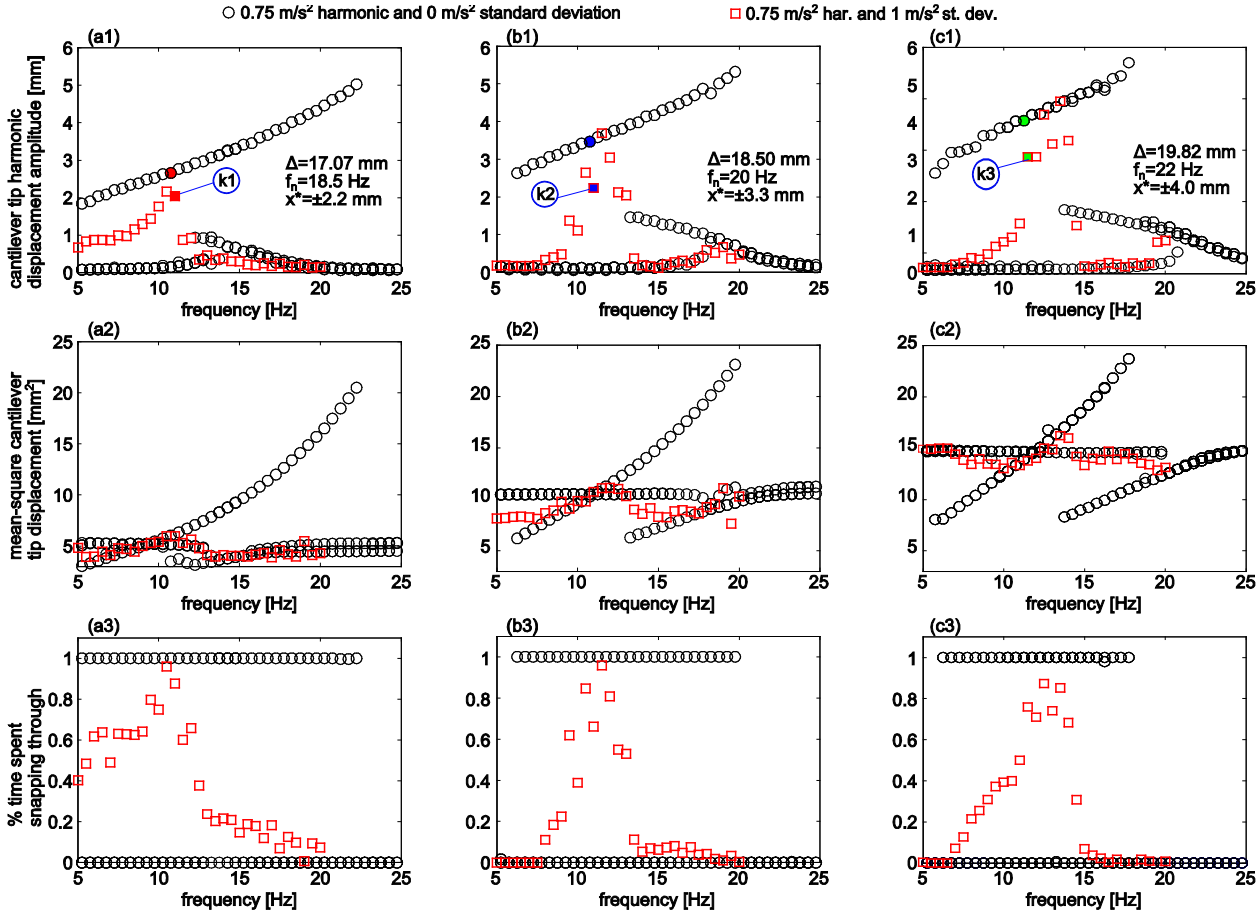

Figure 21. Experimental measurements of bistable structure response as a function of variation in the harmonic excitation frequency for different magnet spaces. Here, harmonic displacement amplitudes are shown in the first row, mean-square displacement in the second row, and percentage of time that the beam spends snapping through per 30-second stationary excitation in the third row. From left to right columns, an increasing distance between the stable equilibria is induced by increasing the magnet positioning parameter Δ .

In addition, as the structural parameters change, the linear natural frequencies of the bistable beam also change. When the magnet space is Δ=17.05mm, and Δ=19.82mm, the locally linear natural frequency of beam oscillations around a stable equilibrium is about 18.5 Hz and 22 Hz, respectively. The increasing magnet space causes the bistable beam to become stiffer, according to this change in natural frequency. Once the stochastic excitation is introduced to the harmonic component, the change in the magnet space parameter plays important roles on the bistable structure dynamics. For instance, the peak displacement amplitude and percentage snap-through time occur at steadily increasing frequencies values as the magnet space increases, shown by red squares in the Fig. 21 first and third row. The highest displacement amplitude and percentage snap-through time for magnet space Δ=17.05mm, and Δ=19.82mm, happen when harmonic frequencies are about 10.5 Hz and 14 Hz respectively. These frequencies are about 55% of the beam linear natural frequencies, which agree with what the observations in section 4.1. Another interesting result is that as the magnet space becomes larger the maximum beam displacement amplitude also increases under the combined harmonic and stochastic excitation, shown by red squares in Fig. 21.

According to experimental results, when magnet space is small Δ=17.07mm, the beam maximum displacement amplitude is about 2.2mm, as shown in Fig 21(a1); when magnet space is in middle level, Δ=18.50mm, maximum displacement amplitude increases to about 3.3mm, as shown in Fig 21(b1); when magnet space further increase to Δ=19.82mm, the maximum beam displacement becomes around 4.0mm, as shown in Fig 21(c1). These results provide evidence that the structural parameter tuning of the symmetric magnet space defines the harmonic frequency band wherein the bistable structure has the greatest displacement amplitude under combined harmonic and stochastic excitation, as well as how large the peak displacement amplitude will become.

Additional examinations of the beam displacement responses in time series at 11 Hz give complementary conclusions to these results. Figure 22 shows snapshots of time series measurements corresponding to (black dashed) steady-state snap-through oscillations without noise and (red dash, blue dot-dash, and green solid) the harmonic and stochastic vibrations when the noise contributes to the excitation for three different magnet spaces, corresponding to the k1, k2, and k3 labels in Fig. 21.

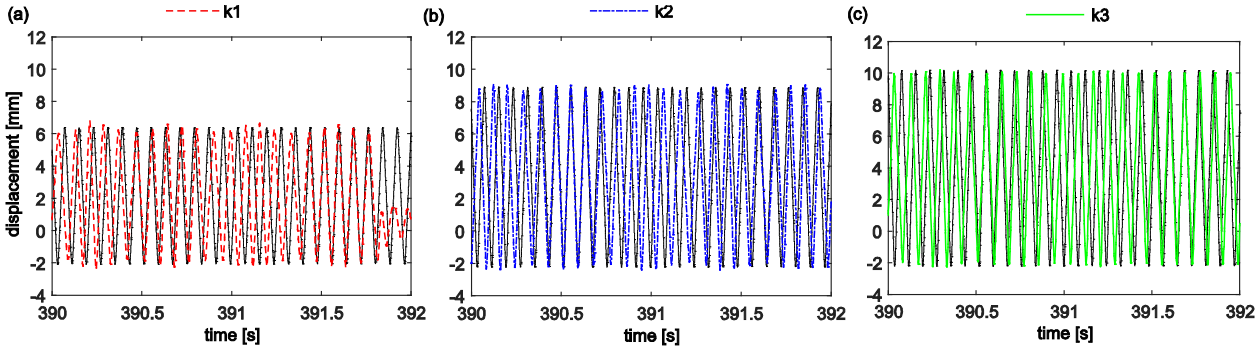

Figure 22. Snap-shot of time series of displacements under harmonic excitation without (black dash) additive noise and with noise (red dash/ blue dot-dash/ green solid). Here, harmonic excitation amplitude is 0.75 m/s2 at 11Hz, (a) corresponds magnet space at Δ=17.07mm (b) corresponds magnet space at Δ=18.50 mm (c) corresponds magnet space at Δ=19.82mm.

According to the results, the additive stochastic excitation component perturbs responses from steady state. Thus, responses shown by trajectories k1, k2 and k3 in Fig. 22 exhibit phase changes compared to the steady-state snap-through. In addition Fig. 22 demonstrates apparent increasing displacement amplitude as the magnet space increases. Although the harmonic displacement amplitudes are different, k1, k2 and k3 still show very large likelihood to snap-through and reveal dynamics dominated by the harmonic excitation frequency. This is shown by the phase portrait and autospectrum in Fig. 23(a), (c). Besides the growing displacement amplitudes due to the increasing magnet space, the responses also show a lower time-varying similarity for larger magnet space, which is proved by the autocorrelation in Fig. 23(b) with a less sinusoidal-like trend.

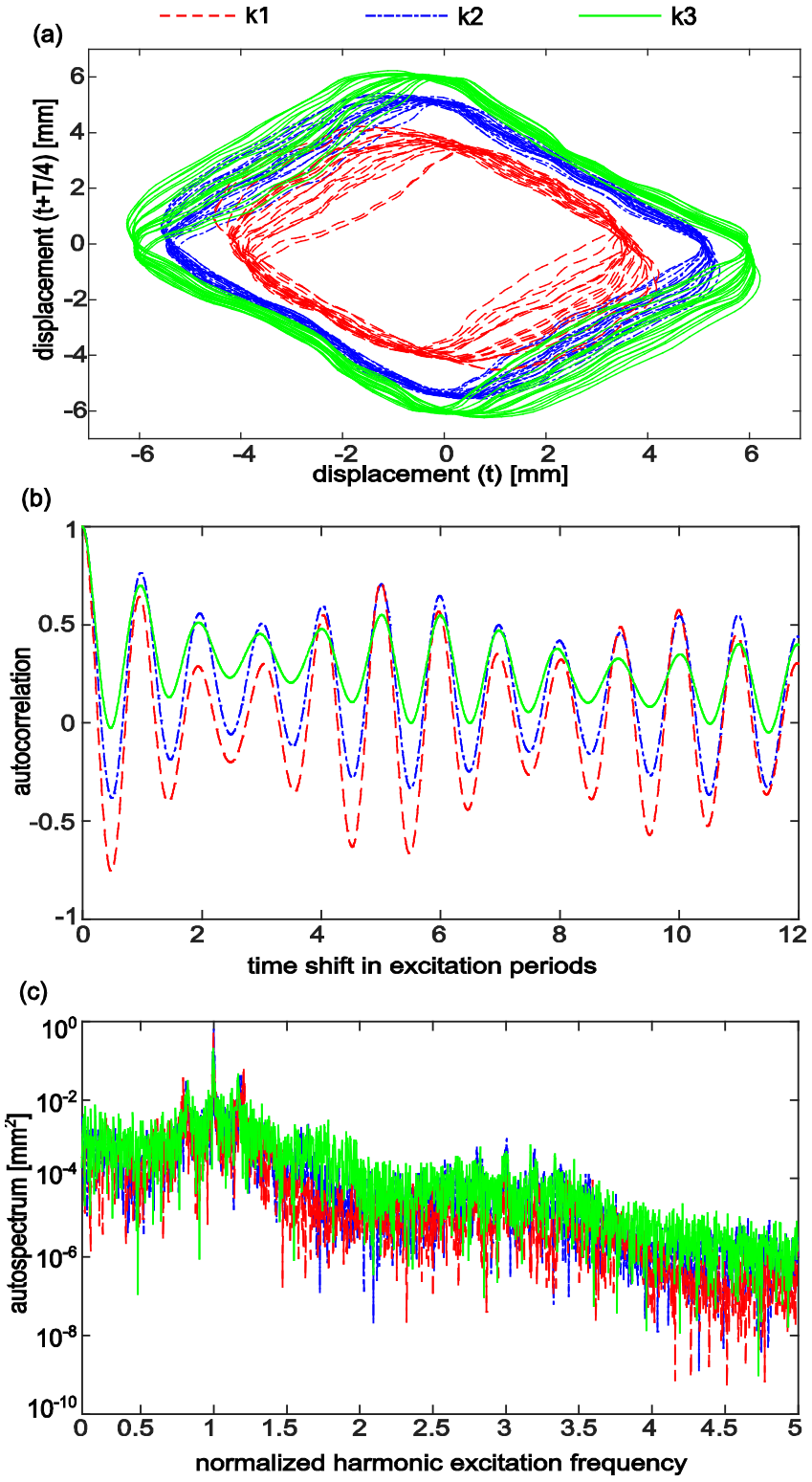

Figure 23. Portions of time series recordings of beam displacement as indicated by the labels k1, k2, and k3, from Fig. 21 under harmonic excitation amplitude 0.75 m/s^2 at 11 Hz, for three different magnet spaces. Here, (a) shows a phase-lag phase portrait of the beam displacement response (b) shows the autocorrelation, while (c) shows the autospectrum of the corresponding data point.

According to these findings, although snap-though dynamics with larger magnet space show larger displacement amplitude, they demonstrate lower response similarity for increasing time shifts in the excitation period. In this way, the increase in magnet space reduces the repeatability of the snap-through response at the same excitation frequency which may be a sign of susceptibility of this snap-through steady-state perturbations.

4.5 Impacts of offset distance: asymmetric bistability

Finally, the roles of asymmetric structural design upon the dynamics sensitivities of the bistable structure are explored by varying the magnet offset distance ε. Previous research are based on the premise that the structure is symmetric, although in practice even the smallest offset distance (or structural imperfection caused by inevitable uncertainties in design) cause noticeable asymmetric dynamic responses [20]. Based on the setup of the archetypal bistable structure in this research, asymmetric system configurations and hence dynamics are introduced by application of non-zero magnet offset distance ε.

The influences of offset distance, ε, upon the steady-state dynamic responses of the archetypal bistable structure are examined in Figure 24 by black circles, blue diamonds and green squares, corresponding to snap-through and two intrawell dynamics, respectively, under sweep harmonic frequency excitation. Harmonic excitation amplitude is set to be 0.75 m/s^2, while harmonic frequency is slowly swept. Results with small magnet asymmetric offset distance are shown in the first column in Fig. 24, as (a1) and (a2). Due to the small offset distance, the bistable beam has two different linear natural frequencies, 18.5Hz and 19Hz, with respect to two stable equilibrium positions, around which bistable beam has intrawell dynamics that is represented by the small displacement amplitude branches in Fig. 24(a1). Since the offset distance is small, the difference between intrawell dynamics around two different stable equilibria is noticeable but not substantial. However, as the offset distance becomes larger, a significant difference exists between the two intrawell dynamics as shown in Fig. 24(b1) by blue diamonds and green squares. In this case, the two intrawell dynamics exhibit notably different amplitudes for the same harmonic excitation frequency. Additionally, the local resonant frequencies of the bistable beam change to 12.75 Hz and 23 Hz: more than 10 Hz difference between two local resonant frequencies. These results provide evidence that offset plays a key role in tuning the local linear resonant frequencies of bistable beam as concluded in the previous research [20], thus governing the frequency band around which the two sets of intrawell dynamics may occur, as well as the amplitude difference between two sets of intrawell dynamics.

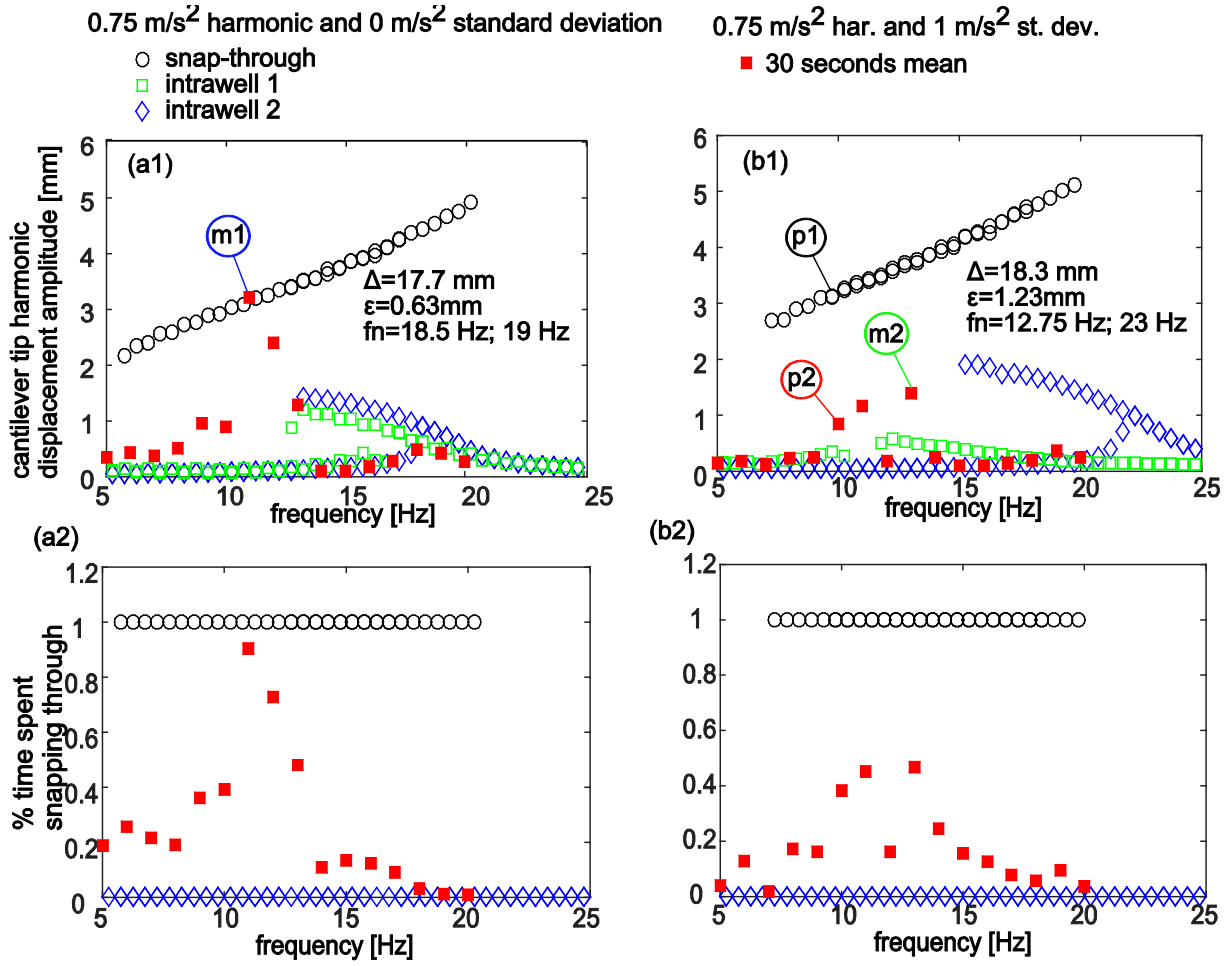

Figure 24. Experimental measurements of bistable structure response as a function of variation in the harmonic excitation frequency for different asymmetric offset distance between the stable equilibria. Here, harmonic displacement amplitudes are shown in the first row, and percentage of time that the beam spends snapping through per 30-second stationary excitation shown in the second row. From left to right columns, an increasing asymmetric offset distance between the stable equilibria is induced by increasing the magnet positioning parameter ε.

The influence of stochastic excitation upon the asymmetric bistable structural dynamics is studied by applying discrete harmonic frequency excitation with noise, such that the harmonic amplitude and noise standard deviation, are 0.75 m/s^2 and 1 m/s^2, respectively. While the harmonic frequency is discretely increased. According to the results shown in Fig. 24(a) by red shaded squares, when magnet offset distance is small, and no noticeable difference between two sets of intrawell dynamics, bistable beam has maximum displacement amplitude and percentage time to snap-through at about roughly one half of the linear resonant frequency, which is comparable to the discovery of Section 4.1. The results after the increase in offset distance to ε= 1.23mm are shown in Fig. 24(b) by red squares. In agreement with the previous observations, the bistable structure appears to have the greatest displacement amplitude when the harmonic excitation frequency is about one-half of the structural local resonance frequency. Also, it is seen that when harmonic excitation frequency is around the local resonance frequency, the likelihood to maintain snap-through responses is significantly compromised. Here, when offset distance ε= 1.23mm,

two local resonant frequencies occur around 12.75 Hz and 23 Hz, one is about the half of the other. Thus when harmonic excitation frequency is about 13 Hz, close to one of the linear resonance frequencies, 12.75Hz, and also close to one half of the other linear resonance frequency 23 Hz, the bistable structure response still has a maximum displacement amplitude, as shown in Fig. 24(b). However, comparing with the maximum amplitude with small offset distance, the value is significantly reduced after increases in the offset distance.

In order to further investigate the bistable structure responses with large offset distance, the time series responses according to labeled points p1 and p2 in Fig. 24(b) are shown in Fig. 25 as persistent snap-through (black dash) and aperiodic dynamics (red solid), respectively. For aperiodic dynamics, a substantial phase change occurs when the beam snaps though, such that it is not consistently in line with the harmonic excitation component. This is evidence that snap-through dynamics with resulting from a strongly asymmetric bistable structure design are significantly perturbed by the stochastic excitation component and are not robust.

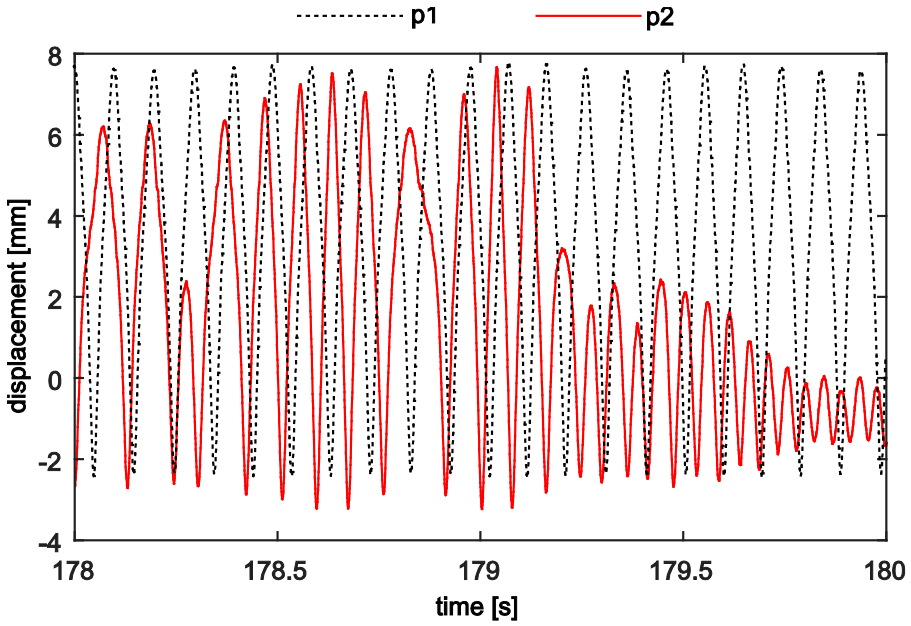

Figure 25. Time series of displacements measured without (black dash) and with (red solid) additive noise under harmonic excitation amplitude 0.75 m/s^2 at 10Hz, with large offset ε= 1.23mm.

More insight is gained by considering the phase-lag phase portrait and autocorrelation of the beam displacement responses with the largest displacement amplitude for small and large offset distance, as shown in Fig. 26, corresponding to labeled points m1 and m2 in Fig. 24. The green solid trajectory m2 demonstrates that as the offset distance increases, the snap-though response has a displacement bias towards one of the stable equilibria, around 0 mm, meaning it is more likely to generate intrawell oscillation around one stable equilibrium than the other. In contrast, the snap-through response with small magnet space distance, shown by blue dash curves shows a relative symmetric phase portrait without apparent bias between two stable equilibria. In addition, the autocorrelation plot shows m1 trajectory has

a more sinusoid-like form then m2 trajectory, which proves a higher repeatability for snap-though behavior with small offset.

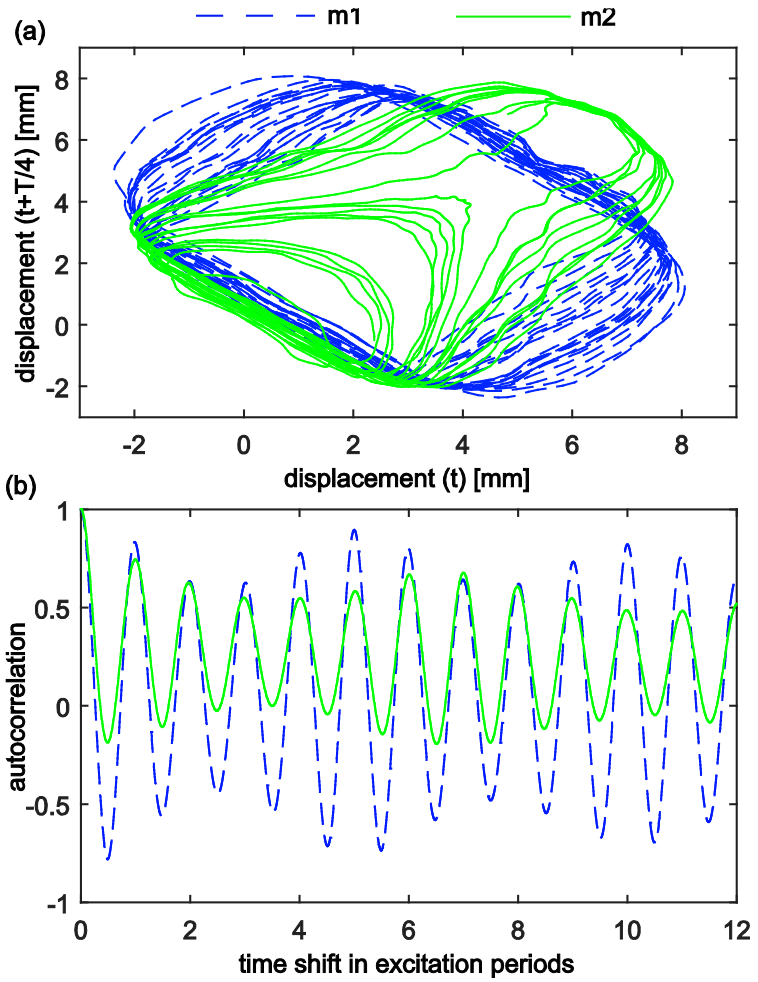

Figure 26. Portions of time series recordings of beam displacement as indicated by the labels m1 and m2, from Fig. 24 under harmonic excitation amplitude 0.75 m/s^2 and noise standard deviation 1 m/s^2, for different offset distance. Here, (a) shows a phase-lag phase portrait of the beam displacement response (b) shows the autocorrelation of the corresponding data point.

Based on these findings, a greater offset distance that leads to noticeable difference between two stable equilibrium configurations from the unstable equilibrium, significantly compromises the robustness and integrity of snap-through dynamics. These findings give insights that in order to reduce the probability to snap-through structures like aircraft panels could be deliberately designed to have significantly asymmetric stable equilibria. While for applications like adaptive structures that want to take advantages of snap-through to tuning properties, one should design them to have relative symmetric stable equilibria.

5 CONCLUSION

Multistability is a structural property that is has great importance in a wide range of applications. For example, it can enhance the performance of adaptive structures, and also may make slender structures

susceptible to undergo large amplitude dynamics thus causing fatigue failure. However, a lack of understanding on the robustness of the dynamics of multistable structures under combined harmonic and stochastic excitations prevents their practical implementation.

Using an archetypal bistable structure that represent a broad kinds of multistable structures, this research experimentally shed lights on the unknown to characterize these sensitivities. The dynamic characteristics of the bistable structure are investigated using different excitation and structural parameter setups under combined harmonic and stochastic excitations. The results of these experimental studies provide guidelines to design and implement multistable structures in real world applications.

As newly discovered through these experimental investigations, the persistent periodic snap-through dynamics are rapidly disabled by the additional noise excitation when the harmonic excitation frequency is around the structural linear resonant frequency. On the other hand, the additional noise also compromises the integrity of the locally stable periodic dynamics by inducing snap-through behaviors in the bistable beam when the harmonic frequency is around one half of the linear resonant frequency.

It is found that under combined harmonic and stochastic excitation, the increasing amplitude of the harmonic component increases the probability for the archetypal bistable structure to generate large amplitude dynamics as well as enhances the robustness of snap-through dynamic. However, when the harmonic excitation level is very low, the response of bistable structure appears to be dominated by oscillations primarily at the fundamental natural frequency.

According to experimental results but also in general agreement with intuition and previous research, noise excitation may perturb the bistable structure from its steady-state dynamics. After the noise level is sufficiently great enough, when compared with the harmonic amplitude, the structure responses undergo occasional transitions from intrawell to large amplitude oscillations or from persistent snap-through to aperiodic snap-through dynamics.

This research found that when the stochastic excitation component perturbs the response from intrawell to large amplitude dynamics, the ratio between the standard deviation of noise and the harmonic excitation amplitude is about 2:1. In contrast, it was discovered that when the response is perturbed from persistent snap-through to aperiodic dynamics, the ratio becomes about the inverse: about 1:2.

The structural parameters, symmetric magnet space and asymmetric offset distance, significantly define the structural properties and the dynamic response. When the magnet pair is set to be ideally symmetric, the increasing magnet space parameter increases the linear resonant frequencies while keeping those two values equivalent. Under combined harmonic and stochastic excitation, as the harmonic frequency discretely increases the bistable structure exhibits the largest displacement amplitude and percentage snap-through time when the harmonic frequency is about one half of the linear resonance. Thus the trends for displacement amplitude and percentage snap-though time shift to right as the symmetric magnet space increases. In addition, the snap-through response has a larger maximum displacement amplitude values and higher response similarity as the symmetric magnet space increases, which is the evidence that snap-through is more robust to noise perturbations. Asymmetric offset distance has a strong impact on the

dynamic responses of the bistable structure. As the offset distance increases from a nearly symmetric condition, the difference of linear resonant frequencies around two stable equilibria positions becomes greater. When the offset is large enough, bistable structure will have a clear bias towards one of two stable equilibria, which compromise the integrity and robustness of snap-through dynamics under combined harmonic and stochastic excitations. Based on these findings, bistable structure is very sensitive to structural symmetry when excited with harmonic and stochastic energies.

The detailed dynamic sensitivities of an archetypal bistable structure under combined harmonic and stochastic excitation is investigated in this research through extensive experimental studies. These findings supplement the knowledge gaps of contemporary research about the dynamic behaviors of multistable structures by using a more real-world like excitation form and a structure commonly encountered throughout engineering applications. The experimental evidence and new conclusions generated here may be used to test analytical models that can be used to predict the potential dynamic responses of multistable structures under different excitation conditions and structural setups. There are many possible applications of this research findings, including appropriately adapt and tune multistable structures as harvesting platforms to increase efficiency, and improve the design of thin aircraft panels to prevent potentially large amplitude dynamics even at extreme working scenario, thus increase the structure lifetime. This research lays a crucial fundament for many specific applications that relate to the implication of structures with more than one equilibria position.

BIBLIOGRAPHY

[1] L. Virgin, Introduction to Experimental Nonlinear Dynamics, Cambridge: Cambridge University Press, 2000.

[2] F. Moon and P. Holmes, "A magnetoelastic strange attractor," *Journal of Sound and Vibration,* vol. 65, pp. 275-296, 1979.

[3] A. Przekop, S. Rizzi and K. Sweiter, "An investigation of high-cycle fatigue models for metallic structures exhibiting snap-through response.," *International Journal of Fatigue,* vol. 021009, p. 136, 2008.

[4] R. Wiebe, L. Virgin, I. Stanciulescu and S. Spottswood, "On snap-through buckling," in *Structural Dynamics and Materials Conference,* Denver, Colorado, 2011.

[5] Z. Bažant and L. Cedolin, Stability of Structures: Elastic, Inelastic, Fracture, and Damage Theories, Hackensack, New Jersey: World Scientific Publishing Co., 2010.

[6] C. McInnes, D. Gorman and M. Cartmell, "Enhanced vibrational energy harvesting using nonlinear stochastic resonance," *Journal of Sound and Vibration,* vol. 318, pp. 655-662, 2008.

[7] S. Zhao and A. Erturk, "On the stochastic excitation of monostable and bistable electroelastic power generators: relative advantages and tradeoffs in a physical system," *Applied Physics Letters,* vol. 102, p. 103902, 2013.

[8] R. Harne and K. Wang, "Prospects for nonlinear energy harvesting systems designed near the elastic stability limit when driven by colored noise," *ASME Journal of Vibration and Acoustics,* vol. 136, p. 021009, 2014.

[9] R. Harne, M. Thota and K. Wang, "Concise and high-fidelity predictive criteria for maximizing performance and robustness of bistable energy harvesters," *Applied Physics Letters,* vol. 102, p. 053903, 2013.

[10] P. Chen and M. Mignolet, "Fatigue life of composite structures in extreme environments," 2005.

[11] C. Ng and S. Clevenson, "High-intensity test of a thermally stresses plate," vol. 28, no. 4, pp. 275-282, 1991.

[12] C. Ng, "Nonlinear and snap-through response of curved panels to intense acoustic excitation," *J. aircraft,* vol. 26, no. 3, pp. 281-289, 1989.

[13] R. Wiebe and Spottswood, "Co-existing resonses and stochastic resonance in post-buckled structures: A combined numerical and experimental study," *Journal of sound and vibration,* no. 333, pp. 4682-4694, 2014.

[14] L. Gammaitoni, P. Hänggi, P. Jung and F. Marchesoni, "Stochastic resonance," *Review of modern physics,* vol. 70, no. 1, pp. 223-288, 1998.

[15] W. Szemplińska-Stupnicka and J. Rudowski, "Steady states in the twin-well potential oscillator: computer simulations and approximate analytical studies," *Chaos,* vol. 3, pp. 375-385, 1993.

[16] L. Virgin, "The dynamics of symmetric post-buckling," *International Journal of Mechanical Sciences,* vol. 27, pp. 235-248, 1985.

[17] M. Daqaq, "Transduction of a bistable inductive generator driven by white and exponentially correlated Gaussian noise," *Journal of Sound and Vibration,* vol. 330, pp. 2554-2564, 2011.

[18] J. Turner and A. Pretlove, "A study of the spectrum of traffic-induced bridge vibration," *Journal of Sound and Vibration,* vol. 122, pp. 31-42, 1988.

[19] P. Bearman, "Vortex shedding from oscillating bluff bodies," *Annual Review of Fluid Mechanics,* vol. 16, pp. 195-222, 1984.

[20] N. Kidambi, R. Harne and K. Wang, "Adaptation of energy dissipation in a mechanical metastable module excited near resonance," *Journal of Vibration and Acoustics,* vol. 138, p. 011001, 2016.

[21] L. Virgin, Vibration of Axially Loaded Structures, Cambridge: Cambridge University Press, 2007.

[22] J. Roberts and P. Spanos, Random vibration and statistical linearization, New York: Wiley, 1990.

[23] R. Wiebe, L. Virgin, I. Stanciulescu, S. Spottswood and a. T. Eason, "Characterizing dynamic transitions associated with snap-through: a discrete system.," *Journal of Computational and Nonlinear Dynamics*, vol. 011010, p. 8, 2013.

6 APPENDIX

6.1 Sample MATLAB code

Below is the sample MATLAB code, using data acquisition toolbox, to generate sweep harmonic frequency analog output signals to control the electrodynamic shaker and take analog input signals from sensors simultaneously. The post processing is also included in the same DAT file.

```
%% Quanqi Dai
%% May 2016

clear all
warning off

%%%%%%%%%%%%%%%%%%%%% start with define parameters and basic variable setting

%% acquire data?
dataacquire=1; % yes for acquire

%% generate output signal?
signalgenerate=1; % yes=1 for generate analog output signal

%% structural parameters
d.del_spacing=2.0574-2.9464; % delta space bwtween magnets [mm](initial value
2.9464mm)
d.mag_spacing=18.5+d.del_spacing; % space between two magnets [mm]

%% analog output setup parameters
d.freq_max=20; % analog output sine max frequency [Hz]
d.freq_min=5; % analog output sine min frequency [Hz]
d.freq_inc=1; % analog output sine frequency increment [Hz]
d.sin_amp=3.5; % [V]analog output sine amplitude
d.seconds=30; % analog output time duration [s]
d.noise_amp=0.08; % analog output noise amplitude
d.filter_lo=1; % [Hz] low-pass filtering frequency on all analog output time
series
d.filter_hi=300; % [Hz] high-pass filtering frequency on all analog output
time series
d.filter_data_lo=1; % [Hz] low-pass digital filter frequency
d.filter_data_hi=200; % [Hz] high-pass digital filter frequency
d.filenum=1; % file number when conducting more than one

%% data acquisition setup parameters
d.fs=2048; % sampling frequency [Hz]
d.wind=@hann; % windowing for averages

%% filename for save d structure
filename=['bistable_beam_sinamp_' num2str(d.sin_amp) '_fixedfreq_noiseamp_'
num2str(d.noise_amp) '_magspace_' num2str(d.mag_spacing) '_'
num2str(d.filenum) '.mat'];
saveon=1; % save the data? NOTE THAT OVERWRITE IS POSSIBLE if filename
already exists in working directory

%% sensor sensitivity
```

```
d.ch_sens(1)=(1/.0979)*9.81; % g/V  % PCB 352C33 accelerometer
d.ch_sens(2)=20; % mm/V % MicroEpsilon ILD-2300 laser displacement sensor
d.ch_sens(3)=20; % mm/V % MicroEpsilon ILD-1700 laser displacement sensor
d.ch_sens(4)=1;

%% mean sensor values
d.data_mean(1)= 0.004271573895005 ; % mean acceleramitor voltage [V]
d.data_mean(2)= 5.168724017496299; % mean ILD-2300 laser displacement sensor
voltage [V]
d.data_mean(3)= 5.710213950593222; % mean ILD-1700 laser displacement sensor
voltage [V]
d.data_mean(4)= 1.041238416069624; % mean switch chanel voltage [V]


%% generate analog output sweep frequency sine signal
d.time_dur=0:1/d.fs:d.seconds-1/d.fs; % generate time duration vector [s]
d.freq=d.freq_min:d.freq_inc:d.freq_max; % frequency generate for output
signal
dd.signal(:,1)=d.sin_amp*sin(2*pi*d.freq(1)*d.time_dur); % starting signal
dd.phase=0; % start total phase is initially zero
d.time_all=d.time_dur; % first total time is first time duration
for sss=2:length(d.freq) % for every frequency
d.time_dur=d.seconds*(sss-1):1/d.fs:d.seconds*(sss)-1/d.fs; % current time
duration
d.time_all((sss-1)*d.fs*d.seconds+1:sss*d.fs*d.seconds)=d.time_dur; %
concatenating time vector
dd.phase(sss)=dd.phase(sss-1)+asin(sin(2*pi*d.freq(sss-1)*d.seconds)); %
start total phase of current signal
dd.signal(:,sss)=d.sin_amp*sin(2*pi*d.freq(sss)*d.time_dur-dd.phase(sss));  %
current signal span
end
dd.signal=reshape(dd.signal,d.fs*d.seconds*length(d.freq),1);% concatenate
signal


%% fft computation parameters
d.sweep_rate=(d.freq_max-d.freq_min)/(d.seconds*(length(d.freq)-1)); %[Hz/s]
sweep rate (ASSUMES SYMMETRY in SWEEP BELOW!)
d.freq_spacing=d.freq_inc; % [Hz] spacing of output frequencies
d.spacing_cts=round(d.fs*d.freq_spacing/d.sweep_rate); % number of samples to
use in FFT to obtain freq_spacing
d.fft_numbers=floor(d.fs*d.seconds*length(d.freq)/d.spacing_cts); % number of
ffts to compute/loop through
d.nft=2^nextpow2(d.spacing_cts); % number of samples next to power of 2 for
spacing_cts

%% adjust signal for shaker constant acceleration according to pre-measured
nonlinear shaker response trends
load('shaker_accel_const_gain_adjust_2_250_hz.mat'); % 2 to 250 Hz
temp_freq=linspace(2,250,max(size(shaker_accel_const_gain_adjust_2_250_hz)));
% generate temporary frequency vector [Hz] according to size of shaker gain
data
mp_freq,flipud(shaker_accel_const_gain_adjust_2_250_hz),dd.f_down);
for sss=1:length(d.freq)
    ind=max(find(temp_freq<=d.freq(sss)));
```

```
    dd.signal((sss-1)*d.fs*d.seconds+1:sss*d.fs*d.seconds)=dd.signal((sss-
1)*d.fs*d.seconds+1:sss*d.fs*d.seconds)*shaker_accel_const_gain_adjust_2_250_
hz(ind);
end

%% adjusting signal amplitudes for up and down and concatenating total
sinusoidal sweep
d.signal_total_adj=0.1*dd.signal; % total out put sine [V]

%% generate noise
d.noisy_signal=d.signal_total_adj+d.noise_amp*randn(size(d.signal_total_adj))
; % add noise to analog output signal

%% filter
myfilt=designfilt('bandpassiir','filterorder',2,'HalfPowerFrequency1',d.filte
r_lo,'HalfPowerFrequency2',d.filter_hi,'samplerate',d.fs);
d.ao_filt=filtfilt(myfilt,d.noisy_signal);
figure(2)
plot(d.time_all,d.ao_filt); % plot analog output signal
xlabel('time [s]');
ylabel('amplitude');

%%%%%%%%%%%%%%%%%%%%%%%%%%%%%% data acquisition toolbox NI

%% if for data acquisition
if dataacquire==1 % 1=yes for acquire

%% identify connected devices
devices=daq.getDevices;

%% acquire data only
if signalgenerate==0
s=daq.createSession('ni');
s.addAnalogInputChannel('Dev3',0,'Voltage'); % add input channels
s.addAnalogInputChannel('Dev3',1,'Voltage');
s.addAnalogInputChannel('Dev3',2,'Voltage');
s.Rate=d.fs; % set output and measuring frequency [Hz]
[d.data,d.time_series]=s.startForeground;

%% bandpass filter data
clear ch_f
d.nn_chan=min(size(d.data));
myfilt=designfilt('lowpassiir','filterorder',4,'passbandfrequency',d.filter_d
ata_hi,'PassbandRipple',0.01,'samplerate',d.fs);
for iii=1:d.nn_chan
ch_f(:,iii)=filter(myfilt,d.data(:,iii)); %
d.data_mean(iii)=mean(d.data(:,iii)); % mean voltage of chs
end
end

%% output signal and acquire data
if signalgenerate==1
s=daq.createSession('ni');
s.addAnalogInputChannel('Dev3',0,'Voltage'); % add input channels
s.addAnalogInputChannel('Dev3',1,'Voltage');
```

```
s.addAnalogInputChannel('Dev3',2,'Voltage');
s.addAnalogInputChannel('Dev3',3,'Voltage');
s.addAnalogOutputChannel('Dev3','ao0', 'Voltage'); % add output channel
outputData=d.ao_filt;
s.queueOutputData(outputData);
s.Rate=d.fs; % set output and measuring frequency [Hz]
[d.data,d.time_series]=s.startForeground;
d.nn_chan=min(size(d.data));

%% bandpass filter data
clear ch_f
d.nn_chan=min(size(d.data));
myfilt=designfilt('lowpassiir','filterorder',4,'passbandfrequency',d.filter_d
ata_hi,'PassbandRipple',0.01,'samplerate',d.fs);
for iii=1:d.nn_chan
ch_f(:,iii)=filter(myfilt,d.ch_sens(iii)*(d.data(:,iii)-d.data_mean(iii))); %
end

%%
end

%%%%%%%%%%%%%%%%%%%%%%%%%%%%%%%% post processing

%% compute fft, tf, psd, coh over averages
est_mean=4; % approximated mean of displacement [mm]
d.data_filt=ch_f; % concatenate filtered data
d.data_filt(:,3)= d.data_filt(:,3)- d.data_filt(:,2); % beam relative
displacement
clear ch_ft gxy gxx coh tf y
for ooo=1:d.fft_numbers; %
    trunc=(ooo-1)*d.spacing_cts+1:ooo*d.spacing_cts; % define truncation in
time
    d.freq_instavg(ooo)=d.freq(ooo); % [Hz] mean instantaneous excitation
frequency
    for iii=1:d.nn_chan
    d.inst_mean(ooo,iii)=mean(d.data_filt(trunc,iii)); % mean of
instantaneous data stream for the channel
    y(:,iii)=fft(d.data_filt(trunc,iii),d.nft)/(d.spacing_cts); % take fast
fourier transform of data
    ch_ft(:,iii,ooo)=2*abs(y(1:d.nft/2+1,iii)); % magnitude of single-sided
fourier transform
    d.f_ft=d.fs/2*linspace(0,1,d.nft/2+1)'; % define frequency vector
    gxx(:,iii,ooo)=y(:,iii).*conj(y(:,iii))/2; % auto power spectrum
    gxy(:,iii,ooo)=y(:,1).*conj(y(:,iii))/2; % cross power spectrum
    d.meansq(iii,ooo)=mean((d.data_filt(trunc,iii)-d.inst_mean(ooo,iii)).^2);
% mean-square system response [units]^2, with mean eliminated
    d.meansq(iii,ooo)=mean((d.data_filt(trunc,iii)-est_mean).^2); % mean-
square system response [units]^2, with mean eliminated
    [d.corr(:,iii,ooo),d.lags]=xcorr(d.data_filt(trunc,iii)-
d.inst_mean(ooo,iii),d.data_filt(trunc,iii)-d.inst_mean(ooo,iii),'unbiased');
% autocorrelation of the signal
    end

     d.snap_cts(ooo,3)=0; % initial snap number
    for ppp=1:length(trunc)-1 % for every data point
```

```
        if d.data_filt(trunc(ppp),3)>est_mean &&
d.data_filt(trunc(ppp+1),3)<est_mean % cross cutoff amp downwards
         d.snap_cts(ooo,3)=d.snap_cts(ooo,3)+1; % count snap number
        end
        if d.data_filt(trunc(ppp),3)<est_mean &&
d.data_filt(trunc(ppp+1),3)>est_mean % cross cutoff amp upwards
         d.snap_cts(ooo,3)=d.snap_cts(ooo,3)+1; % count snap number
        end
    end
d.snap_cyc(ooo,3)=d.snap_cts(ooo,3)/(d.freq_instavg(ooo)*(d.time_series(trunc
(end))-d.time_series(trunc(1)))); % number of snap-through cycles per forcing
cycle

    ind=max(find(d.f_ft<=d.freq_instavg(ooo))); % index for the average
corresponding to the instantaneous frequency
    d.ch_ft_instavg(ooo,:)=max(squeeze(ch_ft(ind-1:ind+1,:,ooo)),[],1); % the
signals' outputs at this instantaneous frequency [units]
    d.gxx_instavg(ooo,:)=max(squeeze(gxx(ind-1:ind+1,:,ooo)),[],1); % the
signals' outputs at this instantaneous frequency [units]
end


%% count perturbation times
for sss=1:length(d.data_filt(:,3)) % for every data point
    d.per_cts(sss,1)=0; % set initial counting time
if d.data_filt(sss,4)>0.1 % if (perturb beam) push buttom
   d.per_cts(sss,1)=d.per_cts(sss,1)+1; % count perturbation
end
end
for ooo=1:d.fft_numbers %
    trunc=(ooo-1)*d.spacing_cts+1:ooo*d.spacing_cts; % define truncation in
time
    d.per_times(ooo)=sum(d.per_cts(trunc,1)); % count perturbation times
during each truncation of time

d.per_times_norm(ooo)=d.per_times(ooo)/(d.freq_instavg(ooo)*(d.time_series(tr
unc(end))-d.time_series(trunc(1))));
end
```

6.2 Portion of laser displacement sensor instruction manual

Below is portion of the instruction manual for Micro Epsilon ILD-1700 laser and Micro Epsilon ILD-2300 laser, about the measuring range. The type of the sensor used in this research are highted by red squares.

Type	**ILD 1700-**	**2**	**10**	**20**	**40**	**50**	**100**	**200**	**250VT**	**500**	**750**
Measuring range	mm	2	10	20	40	50	100	200	250	500	750
Start of measuring range	mm	24	30	40	175	45	70	70	70	200	200
Midrange (MMR)	mm	25	35	50	195	70	120	170	195	450	575
End of measuring range	mm	26	40	60	215	95	170	270	320	700	950
Linearity	FSO	±0.1 %	±0.08 %					±0.1 %	±0.25 %	±0.08 %	±0.1 %
Resolution [1]	µm	0.1	0.5	1.5	4	3	6	12	50	30	50
Measurement frequency programmable		2.5 kHz (1); 1.25 kHz (1/2); 625 Hz (1/4); 312.5 Hz (1/8)									
Light source (laser diode)		Wave length 670 nm, red, max. power 1 mW, laser class 2									
Permissible ambient light (at 2.5 kHz)		10.000 lx							15.000 lx	10.000 lx	
Spot diameter	SMR	80	110	320	230	570	740	1300	1500	1500	1500
	MMR	35	50	45	210	55	60	1300	1500	1500	1500
	EMR	80	110	320	230	570	700	1300	1500	1500	1500
Temperature stability	% FSO/°C	0.025	0.01						0.025	0.01	

Type ILD 2300-		2	5	10	20	30	40	50	100	200
Measuring range [1]	mm	2 / 2 (.08 / .08)	5 / 2 (.20 / .08)	10 / 5 (.39 / .20)	20 / 10 (.79 / .39)	40 / 20 (1.57 / 79)	40 / 20 (1.57 / .79)	50 / 25 (1.97 / .99)	100 / 50 (3 94 / 1.97)	200 / 100 (1.57 / 3.94)
Start of measuring range	mm	24 / 24 (.94 / .94)	24 / 24 (.94 / .94)	30 / 35 (1.18 / 1 38)	40 / 50 (1.57 / 1 97)	175 / 195 (6.89 / 7.68)	175 / 195 (6.89 / 7.68)	45 / 70 (1.77 / 2.76)	70 / 120 (2 76 / 4.72)	130 / 230 (5.12 / 9.06)
Midrange	mm	25 / 25 (.98 / .98)	26.5 / 25 (1.04 / .98)	35 / 37 5 (1.38 / 1.48)	50 / 55 (1.97 / 2.17)	195 / 205 (6.89 / 8.07)	195 / 205 (6.89 / 8.07)	70 / 82.5 (2.76 / 3.25)	120 / 145 (4.72 / 5.71)	230 / 280 (9.06 / 11.02)
End of measuring range	mm	26 / 26 (1.02 / 1.02)	29 / 26 (1.14 / 1.02)	40 / 40 (1.57 / 1 57)	60 / 60 (2.36 / 2.36)	215 / 215 (8.46 / 8.46)	215 / 215 (8.46 / 8.46)	95 / 95 (3.74 / 3.74)	170 / 170 (6 69 / 6.69)	330 / 330 (13.0 / 13.0)
Linearity	µm	0.6	1.5	2	4	12	12	10	30	60
Resolution (at 20 kHz) [2]	µm	0.03	0.08	0.15	0.3	0.6	0.6	0.8	1.5	3
Measuring rate, programmable		49.02 / 30 / 20 / 10 / 5 / 2.5 / 1.5 kHz (49.02 kHz with reduced measuring range)								
Light source (Laser diode)		Wave length 670 nm, red, max. power 1 mW, laser class 2								
Permissible ambient light		10,000 lx ... 40,000 lx								
Light spot diameter (±10 %)	SMR, µm	55 x 85	70 x 80	75 x 85	140 x 200	230	230	255 x 350	350	1300
	MR, µm	23 x 23	30 x 30	32 x 45	46 x 45	210	210	70 x 70	130	1300
	EMR, µm	35 x 85	70 x 80	110 x 160	140 x 200	230	230	255 x 350	350	1300
Operating temperature		0 ... +50 °C (+32 °F up to +122 °F)								
Storage temperature		-20 ... +70 °C (-4 °F up to +158 °F)								
Protection class		IP 65 (with plugged connection)								
Power supply U_B		24 VDC (11 ... 30 V); P < 3 W								
Measurement value output,		RS422, Ethernet, EtherCAT (selectable)								
Synchronization programmable		Simultaneous or alternating								
Sensor cable (standard)		0.25 m (with cable jack)								
Electromagnetic compatibility		EN 61326-1: 2006-10; DIN EN 55011: 2007-11 (group 1, class B); EN 61 000-6-2: 2006-03								
Vibration (acc. to IEC 60068-2-6)		2 g / 20 ... 500 Hz								
Shock (acc. to IEC 60068-2-29)		15 g / 6 ms / 3 axes								
Weight (with 25 cm cable)		550 g				600 g	600 g	550 g		600 g